

# **Grip on wet interfaces: an experimental study on the role of drainage**

by

**Babette Haitsma Mulier**

In partial fulfilment of the requirements for the degree of

**Master of Science**

in Mechanical Engineering

at the Delft University of Technology.

To be defended publicly on May 25<sup>th</sup>, 2020 at 13.30h.

**Thesis committee**

Dr. Dimitra Dodou

Peter van Assenbergh

Dr. Pouyan Boukany

An electronic version of this thesis is available at

<https://repository.tudelft.nl/>.



**TU Delft**

[This page is left blank intentionally.]

# Grip on wet interfaces: an experimental study on the role of drainage

*Babette Haitsma Mulier\*, Peter van Assenbergh, Dimitra Dodou*

Biomechanical Engineering Department, Delft University of Technology, Mekelweg 2, 2628 CD Delft, The Netherlands

**ABSTRACT:** Drainage of fluid from wet adhesive-substrate interfaces is often mentioned to be an important mechanism in obtaining strong grip. It has been hypothesized that micropatterned adhesives – that contain features (e.g., pillars) separated by channels on their surface – have a better drainage capability compared to unpatterned adhesives. Nevertheless, the fluid flow behavior on micropatterned interfaces has not been analyzed before. In this work, the fluid flow on wet adhesive-substrate interfaces was captured on three focal planes and analyzed in terms of flow direction, flow trajectory and flow velocity. The aspect ratio and spacing ratio of the features on the micropatterned adhesives as well as the stiffness of the substrates were varied. Ultimately, the fluid flow velocity was related to the pull-off and friction forces of the adhesives on the substrates. From the results it appeared that the initiation of drainage through the channels of micropatterned adhesives is likely not the direct cause of changes in flow direction. A straight flow path and a semi-wave flow path are distinguished as the two main flow trajectories of the fluid flow. The flow velocity depends on the flow path width and the separation distance between the adhesive and the substrate: the flow velocity increases with a smaller flow path width, and is higher before than after adhesive-substrate contact was established. The flow velocity did not differ among the substrates, which could be the result of the effects of the stiffness and the wetting capability of the substrates cancelling each other out. Moreover, our results suggest that shear forces increase with a larger channel area and a smaller fluid volume, whereas this is not necessarily the case for pull-off forces. The outcomes of this study can be used to develop surfaces for the generation of strong grip under wet conditions.

**KEYWORDS:** grip, drainage, pull-off, friction, wet interface, micropatterned adhesives

## INTRODUCTION

The foot- and/or toepads of many animals offer inspiration for technical solutions for obtaining strong grip on wet interfaces. Pads of tree and torrent frogs, newts, clingfishes, and insects such as katydids and bush crickets all consist of hexagonal or circular cell arrays that are separated by channels.<sup>1-14</sup> Multiple mechanisms jointly contribute to the grip of these animals at wet interfaces, such as hydrodynamic effects, suction and mechanical interlocking.<sup>15</sup> Capillary forces are long-range attachment forces and dominate at larger separation distances, although the strength of the bonds decreases with increasing

separation distance.<sup>16–19</sup> It has been further argued that the channels on the pads enable drainage of fluid from the interface, and that this process is critical for obtaining strong grip on wet surfaces because it enables dry contact and thus grip via Van der Waals forces.

Many empirical studies have been conducted to mimic the properties of the aforementioned micropatterned animal pad, understand the fundamentals of strong grip on wet surfaces, and ultimately achieve strong grip in wet conditions. This requires insight in the role of several parameters, which apply to four main components of a wet patterned adhesive-substrate system: the two surfaces (substrate and adhesive), the substrate-adhesive interface, and the environment.

In relation to the properties of the two surfaces, studies have shown that, in wet environments, grip is generally stronger on softer surfaces due to their conformability and better dewetting properties, and thus enlarged area of close contact.<sup>13,17,20–24</sup> Others have investigated the effect of the shape and dimensions of the features of the adhesive on pull-off and friction forces in wet environments. For example, it has been shown that a larger spacing ratio – the ratio between the channel width and the center-to-center distance between the features – increases shear forces, whereas small spacing ratios increase pull-off forces in wet environments.<sup>3,5,7,25–28</sup> It has also been shown that a larger aspect ratio – the ratio between the height and width of the features – can result in a reduction of shear forces on wet interfaces.<sup>11,16</sup> The effect of the aspect ratio of the features on pull-off forces has not been systematically investigated in wet environments.

When it comes to the properties of the interface, it has been shown that an increasing fluid volume generally reduces shear and pull-off forces of micropatterned adhesives.<sup>3,8,9,16,17,20,28–32</sup> However, micropatterned adhesives seem to generate higher pull-off forces on wet compared to dry interfaces.<sup>27,28,33–38</sup> This is generally the other way around for friction. The higher pull-off forces on wet interfaces could be due to the presence of capillary forces, which do not act on dry interfaces.<sup>39</sup> Also pattern-specific characteristics can positively contribute to pull-off, such as via a passive suction-effect observed in the case of mushroom-shaped pillars.<sup>34</sup>

Despite of their smaller actual contact area, micropatterned adhesives often generate higher pull-off and shear forces compared to unpatterned adhesives in wet environments.<sup>3,4,12,14,16,20,25,26,33,34,40,41</sup> Some studies have assigned the higher pull-off force of micropatterned adhesives to discontinuous crack propagation, which is induced by independent detachment of the pillars of a micropattern from a surface.<sup>4,42,43</sup> Moreover, in a study, investigating underwater adhesion, Rao et al. have shown that micropatterned adhesives are also more compliant in the contact point, and thus have a higher debonding energy compared to unpatterned adhesives in pull-off measurements.<sup>4</sup> It has also often been argued that the channels facilitate drainage of fluid from the interface, which results in a larger dry-on-dry contact area, and subsequently in higher friction and pull-off forces.<sup>3,4,17,43,44</sup>

Although drainage of fluid from the micropatterned adhesive-substrate interface is often mentioned as main contributor for strong grip under wet conditions, there is lack of fundamental studies that quantitatively map the fluid flow at wet, micropatterned adhesive-substrate interfaces and directly show its relation to pull-off and friction forces. So far, studies have provided insight into the relation between hydrodynamic forces and separation distances between unpatterned and micropatterned adhesives and wet substrates in time.<sup>27,45–50</sup> Namely, hydrodynamic forces appear to increase exponentially when the separation distance decreases. Based on a comparison of the hydrodynamic forces between micropatterned and unpatterned adhesives, and flooded substrates in time while peeling or moving the adhesive from or normal to the substrate, Gupta & Fréchet and Dhong & Fréchet hypothesized that fluid is drained through the channels on the micropatterned adhesives only at distances smaller than a critical separation distance between the adhesive and the substrate.<sup>45,47</sup> Next to validating this hypothesis, studies about the quantitative drainage properties of micropatterned adhesives could give insight in how hydrodynamic forces respond to a maximization of the channel area to facilitate drainage on the one hand, and a maximization of the pillar diameter to increase the initial contact area on the other hand.

In this study, the fluid flow behavior on adhesive-substrate interfaces was captured upon approach of micropatterned and unpatterned adhesives, and related to the gripping performance of the adhesives in terms of pull-off and friction. Substrate stiffness, and aspect ratio and spacing ratio of the features on the micropatterned adhesives were independently varied during the drainage, friction and pull-off measurements. Moreover, the fluid flow was captured on three focal planes of the microscope during the drainage measurements, which enabled mapping the flow distribution in the normal direction as well as in the lateral direction.

The outcomes of this study add to the knowledge of the fundamentals of obtaining strong grip on wet interfaces. This knowledge could lead to improvements in the design of industrial applications as well as daily life products that are operating or used in wet environments. For example, the gripping performance of medical instruments – such as grippers –, robot picker pads, shoe soles, patterned tires or razor blades in wet environments could significantly be enhanced.

## MATERIALS AND METHODS

### Materials and equipment

A foil photomask was ordered from CAD/Art Services (Bandon, OR, USA). SU-8 2075 photoresist was ordered from Microchem (Newton, MA, USA). Developer (Propylene glycol monomethyl ether acetate, PGMEA) was ordered from Merck (Darmstadt, Germany). Release agent trichloro(1H,1H,2H,2H-perfluorooctyl)silane and LB 30 polystyrene latex beads (mean diameter of 3.0 $\mu$ m and density of 1.005kg/L) were ordered from Merck (Darmstadt, Germany). Beads were suspended in demineralized water at 10 w/w% before use. Polyvinyl alcohol (PVA, Selvol PVOH 165; hydrolysis rate: 99.65%  $\pm$  0.35%; degree of polymerization: about 2000, as reported by the manufacturer) was purchased from Sekisui Chemical Group. Poly-dimethoxysiloxane (PDMS, Sylgard 184) base and crosslinker were purchased from Dow Corning, Midland, MI, USA).

### Fabrication methods

#### *Adhesive fabrication*

Three geometrical different micropatterned adhesives and an unpatterned adhesive were fabricated in threefold from PDMS. A silicon wafer was coated with an SU-8 resist layer at a thickness of 55  $\mu$ m, and soft-baked (for 3 minutes at 65  $^{\circ}$ C and for 6 minutes at 95  $^{\circ}$ C) to allow curing. Using a foil photomask, desired patterns were transferred into the resist layer by exposure to UV-light (with an intensity of 15 MJ/cm<sup>2</sup> for 48 s), post-exposure baking (for 5 minutes at 65  $^{\circ}$ C and for 12 minutes at 95  $^{\circ}$ C), cooling down for 10 minutes to 55  $^{\circ}$ C, developing in PGMEA for 10 minutes and a subsequent plasma flash. The wafer contained 1  $\times$  1 cm<sup>2</sup> arrays of squared-packed cylindrical holes with a diameter of ca. 40  $\mu$ m or ca. 80  $\mu$ m and a spacing of ca. 20  $\mu$ m (called henceforth d40s20 and d80s20, respectively), or a diameter of ca. 80  $\mu$ m and a spacing of ca. 40  $\mu$ m (called henceforth d80s40). We define the spacing as the shortest distance between two neighboring holes. The wafer acted as a three-dimensional template in a subsequent molding step. Before use, the wafer was coated with trichloro(1H,1H,2H,2H-perfluorooctyl)silane, acting as an anti-stick layer by oxidizing the wafer surface in a plasma cleaner (Harrick Plasma Cleaner PDC001) for 140 s, and subsequent chemical vapor deposition. PDMS base and curing agent were mixed in a weight-based ratio of 10:1, and the mixture was degassed in a desiccator before use. An aluminum frame,

containing a  $7 \times 7 \text{ mm}^2$ -opening, was placed on the relevant region of the wafer template, and filled with the uncured PDMS mixture. The wafer, with the filled frame on top, was placed in a desiccator to degas the PDMS, and subsequently cured in an oven at  $68 \text{ }^\circ\text{C}$  for 2 hours. The adhesive was retrieved by peeling the cured PDMS from the wafer and frame. This procedure resulted in an adhesive thickness of  $3.5 \text{ mm}$  and an apparent contact area of  $7 \times 7 \text{ mm}^2$ . The exact geometrical properties of the micropatterns on the adhesives that were used in the experiments can be found in Table 1. The unpatterned adhesives were fabricated by following the same procedure as for the micropatterned adhesives, but with the wafer being an uncoated, flat glass slide.

**Table 1.** Geometrical properties of the micropatterned adhesives.

Adhesive pattern	Average actual pillar diameter ( $\mu\text{m}$ )	Average actual pillar spacing ( $\mu\text{m}$ )	Average actual pillar height ( $\mu\text{m}$ )	Actual surface area <sup>a</sup> (%)	Wall area per pillar ( $\mu\text{m}^2$ )	Wall area <sup>b</sup> (%)
d40s20	36.3	24.3	57.2	34.9	6911	52.4
d80s20	77.4	22.0	61.4	50.3	13823	62.8
d80s40	79.6	40.0	55.1	34.9	13823	52.4

<sup>a</sup> Ratio of pillar tip area to total (pillar tip and channel) area. <sup>b</sup> Ratio of pillar perimeter to the perimeter of the pillar plus its spacing.

### Substrate fabrication

A glass and a PDMS hemisphere were used as substrates. The glass substrate was a UV fused silica plano-convex lens (LA4380, Thorlabs Inc., Newton, NJ, USA) with a radius of curvature of  $46.0 \text{ mm}$ , a center thickness of  $3.8 \text{ mm}$  and a Young's modulus of  $E = 73.6 \text{ GPa}$ . The PDMS substrate was fabricated in the same shape as the glass substrate. First, a PDMS negative mold of the glass lens was fabricated by covering the lens with uncured PDMS, degassing, and subsequent curing in an oven at  $68^\circ\text{C}$  for 2 hours. This mold was then oxidized in a plasma oven and coated with trichloro(1H,1H,2H,2H-perfluorooctyl)silane using chemical vapor deposition. Finally, uncured PDMS (base and curing agent were again mixed in a weight-based ratio of 10:1) was casted in the coated mold, degassed, and cured in an oven at  $68 \text{ }^\circ\text{C}$  for 2 hours. This resulted in a Young's modulus of  $E = 580 \text{ kPa}$  for the PDMS substrate according to Park et al.<sup>51</sup> The glass and PDMS substrates were coated with PVA afterwards to reduce the difference in wetting capability between the substrates, following the procedure described by Trantidou et al.<sup>52</sup> Contact angle measurements on the substrates were performed on a Theta Lite Optical Tensiometer with a  $2 \mu\text{L}$ -droplet of deionized water.

### Drainage measurements

#### Setup

A schematic of the setup is presented in Figure 1. The substrate (4), with the curved side facing up, was placed on a glass slide, which was placed in a custom-made aluminum holder (5) that allowed for illumination of the substrate from below (7). The adhesive (3), with the pattern facing down, was positioned above the substrate using a custom-made cantilever (8). The cantilever was attached to two one-axis linear translation stages (9) (Thorlabs PT1/M-Z8, each powered by a KDC101 controller), providing normal and lateral movement of the adhesive with respect to the substrate. The stages had an accuracy of  $\pm 1 \mu\text{m}$  and a backlash of  $25 \mu\text{m}$ .<sup>53</sup> This substrate-adhesive system, including holder, cantilever

and translation stages, was placed on an independently controlled microscopic table (6), allowing for lateral and normal displacement of the complete setup relative to the microscopic lens (1). A more detailed explanation of the setup, a 3D-schematic and drawings of the parts can be found in the Supporting Information (SI; sections S.1.1 and S.1.2). The surroundings had a temperature of  $20.4\text{ }^{\circ}\text{C} \pm 0.32\text{ }^{\circ}\text{C}$  and a relative humidity of  $56.1\text{ \%rh} \pm 1.5\text{ \%rh}$ .

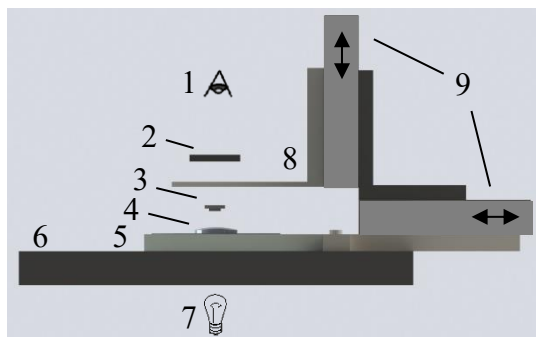


**Figure 1.** Schematic of the side view of the setup for the drainage measurements. An adhesive (3) is placed in a hole in the cantilever (8) and is locked by a lid (2) in normal direction (the adhesive and the lid are exploded for clarity). The adhesive is positioned exactly above a hemispherical substrate (4) that is placed on a glass slide in an aluminum holder (5), which is mounted to the microscopic table (6). The setup is illuminated from below (7) and viewed from above (1). Two linked, linear translation stages (9) provide normal and lateral movement of the cantilever. Their degrees of freedom are indicated by arrows.

The fluid flow was captured with a Keyence VHX6000 microscope, having a magnification of 500x resulting in a field of view of  $502\text{ }\mu\text{m} \times 670\text{ }\mu\text{m}$ . Suspended beads served as flow trackers. The horizontal focal plane at which these particles were captured laid at the tip ( $h = 0\text{ }\mu\text{m}$ ), half-way ( $h = 27.5\text{ }\mu\text{m}$ ), or at the onset ( $h = 55\text{ }\mu\text{m}$ ) of the adhesive's micropillars. Here,  $h$  is the distance between the focal plane and the calibrated contact plane. The fluid flow behavior at the interface of the substrate and the unpatterned adhesive was assessed at the plane of contact. Videos of experiments were recorded by screen capturing, using the Bandicam Screen Recorder (version 4.4.3; 2019).<sup>54</sup> Recorded videos had a resolution of  $1080 \times 1920$  pixels, and included 30 to 40 unique frames per second.

### Experiment sequence

The contact position between adhesive and substrate was calibrated by moving the adhesive towards the substrate in steps of  $5\text{ }\mu\text{m}$ . Upon contact, which was monitored via the microscope, the adhesive was moved an additional  $100\text{ }\mu\text{m}$  downwards to maximize the contact area between adhesive and substrate. This position was set as the calibrated contact position. The field of view of the microscope captured the center of the contact area. The focal plane of the microscope was found by visually examining the light diffraction via the deformed pillars, or – in case of an unpatterned adhesive – by depositing  $0.15\text{ }\mu\text{L}$  of the diluted particle solution to the substrate, and adapting the focal plane of the microscope correspondingly to bring the particles in focus. Then, the cantilever was moved  $6\text{ mm}$  upwards.

The microparticle suspension was mixed with deionized water in a 1:80 (v/v) mixing ratio. A  $10\text{ }\mu\text{L}$ -droplet of this mixture was spread over the patterned side of the adhesive using a flat polystyrene rod until all channels were fully wetted. Another  $100\text{ }\mu\text{L}$  of the diluted particle suspension was then distributed over the substrate. The pre-wetting procedure was not applicable to an unpatterned adhesive. Therefore,  $110\text{ }\mu\text{L}$  of the particle mixture was deposited on the substrate in this case. The adhesive was then moved

down – from an initial separation distance of 1.5 mm to the calibrated contact position – with a velocity of 50  $\mu\text{m/s}$  at an acceleration of 1.5  $\text{mm/s}^2$ . Flow was recorded during approach and up to 30 s after contact.

With the three patterned adhesives and one unpatterned adhesive, two substrates and three focal planes, twenty unique conditions existed. Each condition was tested five times, and all measurements were conducted in a randomized order. Prior to the experiments, the adhesive, substrate and rod were thoroughly cleaned with ethanol and fluttered until they were dry. Scotch Magic Tape was used to remove remaining particles from the adhesives.

### Data analysis

Per experiment, the flow direction, flow trajectory and qualitative flow velocity were extracted from the raw data by visual observation (SI-section S.1.4). The quantitative analysis of the flow velocity was based on four main steps: time synchronization, pre-processing, calculation of particle velocities and post-processing.

First, each unique frame of each experiment was matched with its corresponding point in time and separation distance during the quantitative analysis. The points in time at which the downward movement of the adhesive and the screen capturing started were synchronized per experiment by the MATLAB-script (version 2018b) in SI-section S.1.3.<sup>55</sup> The script also synchronized the time between the two devices on which these sequences were started per day and during the day. The script linearly interpolated between the time at the start and end of each day, because a proportional increase or decrease of the time difference between the two devices along the day was assumed.

The MATLAB-script in SI-section S.1.3 pre-processed the original frames of the screen records (Figure 2). Particles within a particular depth-of-field range were filtered, because the flow was not exactly 2D and the depth of the microscopic field of view was relatively large. For this purpose, unique frames were binarized while a grey value threshold per experiment (varying between 0.585 and 0.615) was set in MATLAB. This threshold was based on visual assessment of the conversion of in-focus particles in the original images to clear pixels in the binary images, and the number of particles that were left in the binary image. Also, masks were applied during pre-processing to cover particles in air bubbles, between the substrate and the pillars on the adhesive, and in particle clusters in the field of view, because these particles were trapped and had no velocity per definition. The position of the masks with respect to the pillars was determined per experiment by manually subtracting the coordinates of the bottom right pillar center and taking the dimensions of the patterns into account. Finally, the images were cropped. The result of data pre-processing is shown in Figure 2.

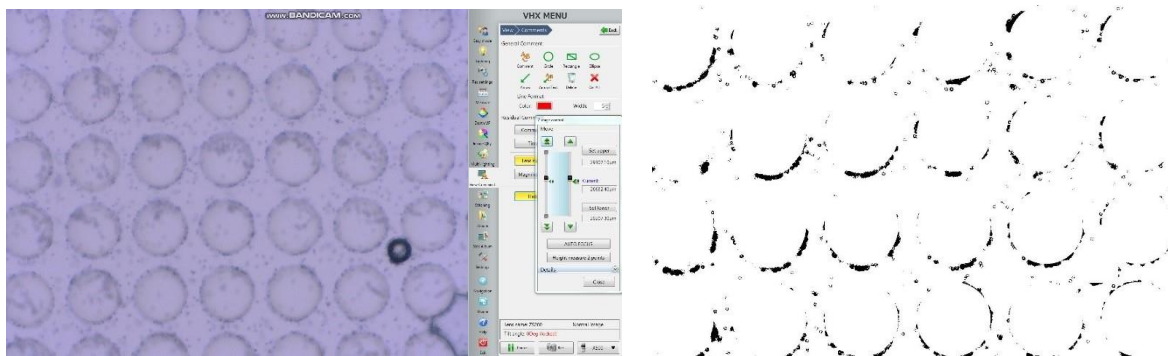


**Figure 2.** An original frame – extracted from the raw data – that is the input for data pre-processing (left), and its binary, cropped equivalent with masks that is the output of data pre-processing (right). The frame depicts a wet d80s20-adhesive on glass with the focal plane half-way of the micropillars.



The average x- and y-velocities of particles within so-called interrogation areas were calculated by analyzing the binary images per subsequent frame. The analysis was based on particle image velocimetry (PIV) for which PIVlab-software (version 7.10 – 8.6) and its default FFT linear window deformation algorithm was used.<sup>56</sup> The size of the interrogation area (pass 1: 64 px, step 32 px; pass 2: 32 px, step 16 px; shown in Figure 3) was based on the number of particles in the area, the particle size, and the smallest channel area among the adhesive patterns.

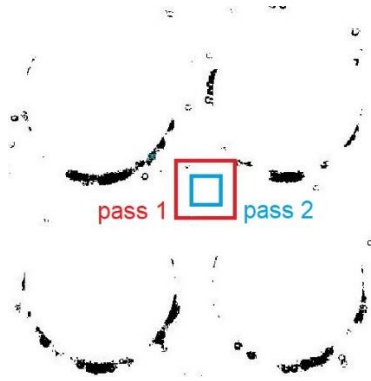


**Figure 3.** Visualization of the size of the interrogation areas in the PIVlab-software relative to four pillars in a binary frame. The adhesive pattern with the smallest spacing relative to the pillar diameter (d80s20) is shown; the focal plane was located half-way of the micropillars.

Finally, the data was post-processed and plots were generated from the velocity data with the MATLAB-script in SI-section S.1.3. Most of the noise in the data plots was removed by a low-pass filter with a pass-band frequency of 5 Hz. An example of the output of the final data processing step without and with a low-pass filter is shown in Figure 4.

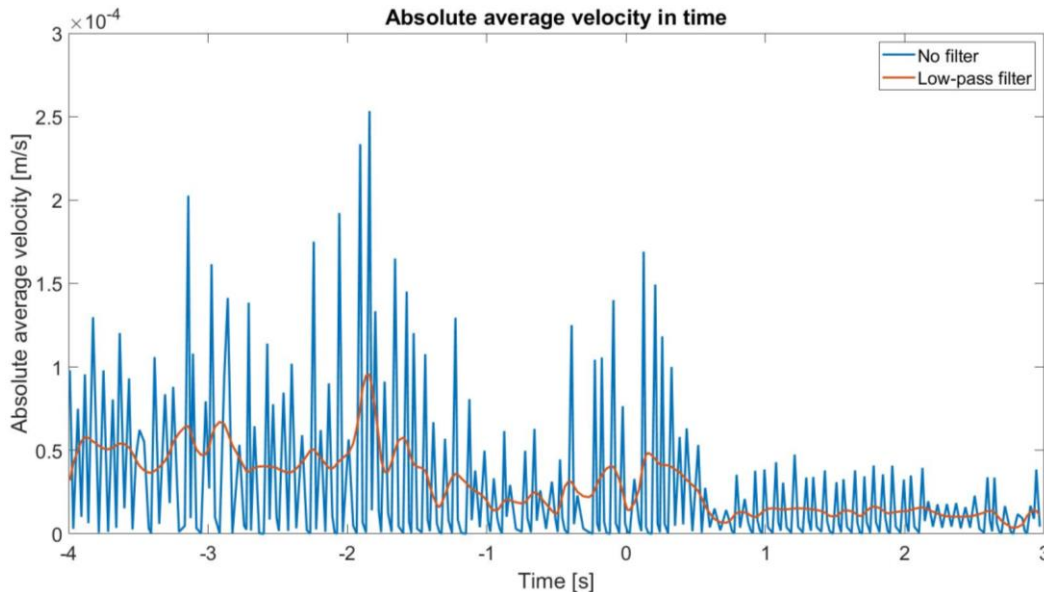


**Figure 4.** Absolute average flow velocity of particles from 4 s before until 3 s after calibrated contact, on an interface consisting of a d80s20-adhesive and glass. The focal plane was located half-way of the micropillars. The plots show the velocity data when no filter is applied and when a low-pass filter with a pass-band frequency of 5 Hz is applied.

## **Pull-off and friction measurements**

### *Setup*

To measure pull-off and friction forces, a custom-built force transducer was used that was presented in earlier work.<sup>57</sup> The substrate was mounted to the force transducer with a custom-made holder (details can be found in SI-sections S.2.1 and S.2.2), which was able to translate in three orthogonal directions due to its suspension by three sets of parallelogram-flexures in series. Two confocal chromatic aberration sensors (CL1 MG210; Stil S.A.S) monitored the displacement of the holder in lateral and normal direction at a measurement frequency of 1000Hz. CCS Manager software (Version 1.5.2.404; Stil) was used to control the sensors by Prima controllers (Stil). The adhesives were cleaned – and in case of patterned adhesives pre-wetted with 10  $\mu\text{L}$  – in the same way as in the drainage experiments, before being placed in a custom-made aluminum cantilever above the substrate with their surface pattern facing down. The cantilever was again laterally and vertically moved by two one-axis linear translation stages (Thorlabs PT1/M-Z8, powered by two KDC101 controllers), having zero overshoot. The temperature and the relative humidity of the surroundings were considered to be constant and 22.4 °C and 38.4 %rh, respectively.

### *Experiment sequence*

First, a 100  $\mu\text{L}$ - or 110  $\mu\text{L}$ -droplet of deionized water (for a patterned or unpatterned adhesive, respectively) was applied and spread over an area near the center of the substrate. The calibrated contact position was found by moving the adhesive in steps of 10  $\mu\text{m}$  towards the wet substrate. When contact was registered by the force transducer, the adhesive was moved another 50  $\mu\text{m}$  towards the substrate to maximize the contact area while preventing the pillars from collapsing during sliding. The adhesive was preloaded like this for 6 s, and the pull-off force was measured by retracting the adhesive over a distance of 1 mm normal to the substrate at a velocity of 100  $\mu\text{m}/\text{s}$  and an acceleration of 4  $\text{mm}/\text{s}^2$ . The channels were then pre-wetted another time with the remaining fluid on the adhesive's surface. After keeping the adhesive in the calibrated contact position for another 6 s, the friction measurement was conducted by laterally moving the adhesive 1 mm at a velocity of 500  $\mu\text{m}/\text{s}$  and an acceleration of 4  $\text{mm}/\text{s}^2$ . Pull-off and friction forces are measured consecutively and repeated 10 times per condition, by randomly alternating the four adhesives and two substrates, so that 80 experiments are conducted in total.

### *Data analysis*

Noise in the captured displacement data was removed with the help of a low-pass Butterworth filter. To generate representative force-time curves, the filtered displacement data was converted into forces by characterization matrices. These matrices contained the stiffness of the platform, and were obtained via a calibration procedure. During the procedure, the platform was loaded independently in lateral and normal direction with 0, 58.9, 108, 157, 206 and 255 mN. The resulting displacement and crosstalk were recorded, and characterization matrices were deduced.

The maximum pull-off force per experiment was manually extracted from the force-time curve (corresponding with the minimum in Figure 7). The maximum (static) friction force corresponded with the point in time on which the adhesive started sliding on the substrate, which was extracted from the displacement-time curve. The MATLAB-scripts that are used to generate the force-time curves and boxplots of the pull-off and friction data can be found in SI-sections S.2.3 and S.2.4.

## RESULTS

### Substrate properties

The average static contact angle was much larger on the coated PDMS substrate ( $94.1^\circ$ ) compared to the coated glass substrate ( $27.0^\circ$ ). Also, it was observed that the droplet was not uniformly distributed on the surface: the fluid layer was thicker near the edge than in the center of the hemispherical substrate.

### Drainage

#### *Flow direction*

The direction of the particle flow differed among measurements of an identical condition (Table S1). The flow direction also often changed within a measurement, for all tested separation distances between adhesive and substrate (Table S2). Next to particles flowing in orthogonal (x- or y-) and non-orthogonal (combined x- or y-) directions as indicated in Figure 5, sometimes the particles flowed radially outwards from the field of view during approach. Also, sometimes all particles in the field of view exhibited simultaneous zigzag moves – fast, short movements on a fixed position without moving in any particular direction – just before contact as if they were trapped between substrate and adhesive.

#### *Flow trajectory*

The observations of the main flow trajectory per experiment can be found in Table S3. The raw data showed that when the particles flowed in one of the orthogonal directions on the pattern (the x- and y- directions as indicated in Figure 5), they followed a straight path in the middle of the channels and a semi-wave path at the edge of the channels, near the pillars. The particles rarely flowed around a pillar. When the particles did not flow in one of the orthogonal directions, the particles followed a semi-wave path (Figure 5). Both semi-wave paths and straight paths occurred in one measurement when part of the particles flowed in an orthogonal direction and part of the particles flowed in a non-orthogonal direction. Particles flowed around trapped air regions when the latter were in the same plane as their flow path.

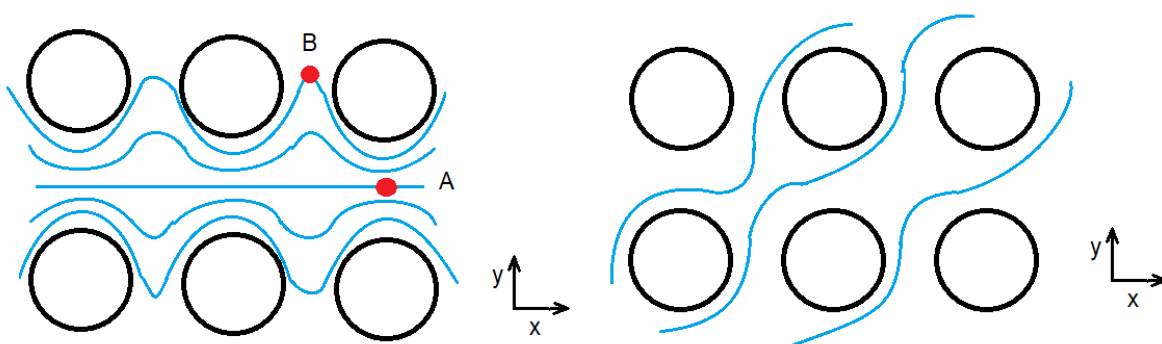


**Figure 5.** Schematic of typical flow trajectories. (Left) Particles flowing in one of the orthogonal directions on the pattern. Particles in the middle of the channels follow a straight path (point A), whereas particles at the side of the channels follow a semi-wave path and have a lower velocity (point B). (Right) Particles flowing in one of the non-orthogonal directions follow a semi-wave path.

### Flow velocity – qualitative

In most cases, drainage took place during approach. In the orthogonal flow direction, particles in the middle of the channels seemed to have a higher velocity compared to particles at the side of the channels. Moreover, as the width of the flow path constantly changed over its length, particles were accelerated when the flow path width became smaller (e.g., at point A in Figure 5) and particles were decelerated when the flow path width increased (e.g., at point B in Figure 5). When the adhesive almost reached the calibrated contact position, the flow often either abruptly stopped or quickly slowed down. Before this happened, the direction of the flow often abruptly changed (often opposite to its initial direction). Sometimes the particles were not abruptly stopped or quickly slowed down when the adhesive stopped moving. On all unpatterned adhesives, and occasionally on patterned adhesives, no flow is observed. The observations of the flow direction, and remarkable changes in flow direction and flow velocity per experiment can be found in Table S1.

### Flow velocity – quantitative

The graph in Figure 6 allows for a comparison of the particle velocity among all repetitions of the experiments on glass and PDMS, with a d80s20-adhesive and the focal plane half-way of the micropillars. The adhesive reached the calibrated contact position at 0 s.

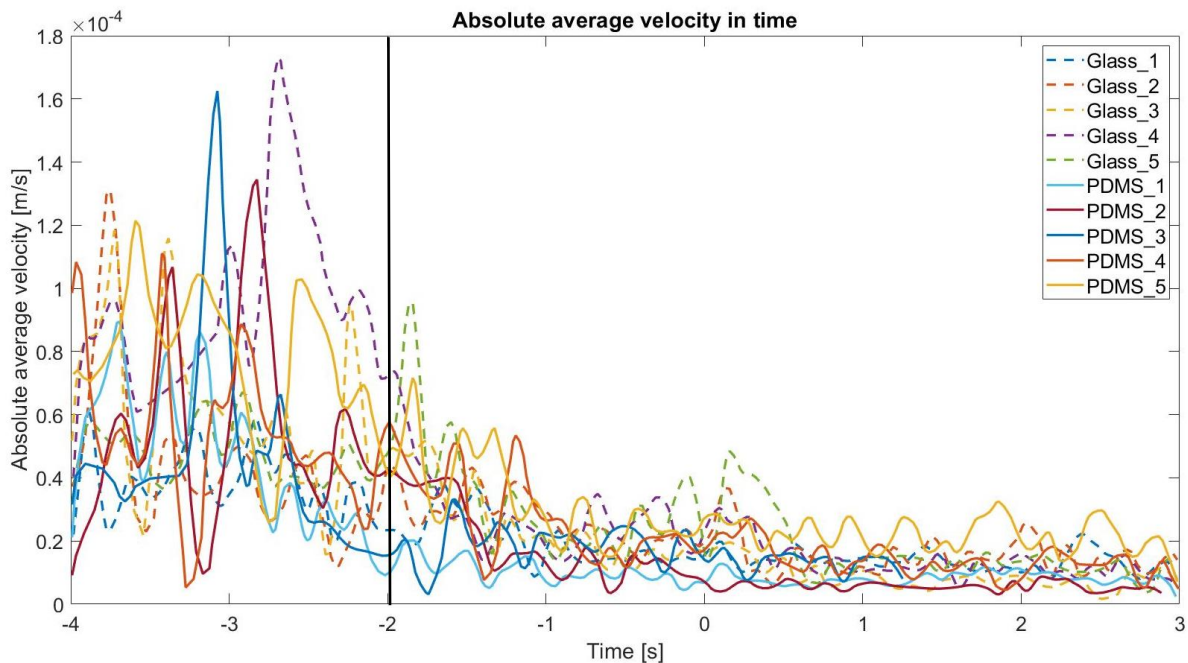


**Figure 6.** Plot of the absolute average flow velocity of the particles in time, of the five repetitions of two experiment conditions: a d80s20-adhesive on glass and PDMS, with the focal plane half-way of the micropillars. The initial adhesive-substrate contact was established at  $t = -2$  s (indicated); the moment at which the adhesive reached the calibrated contact position coincides with  $t = 0$  s.

## Pull-off

Representative force-time plots of pull-off measurements of micropatterned adhesives from glass and PDMS are shown in Figure 7. The maximum pull-off force (phase III) is clearly distinguishable on PDMS, but often not on glass.

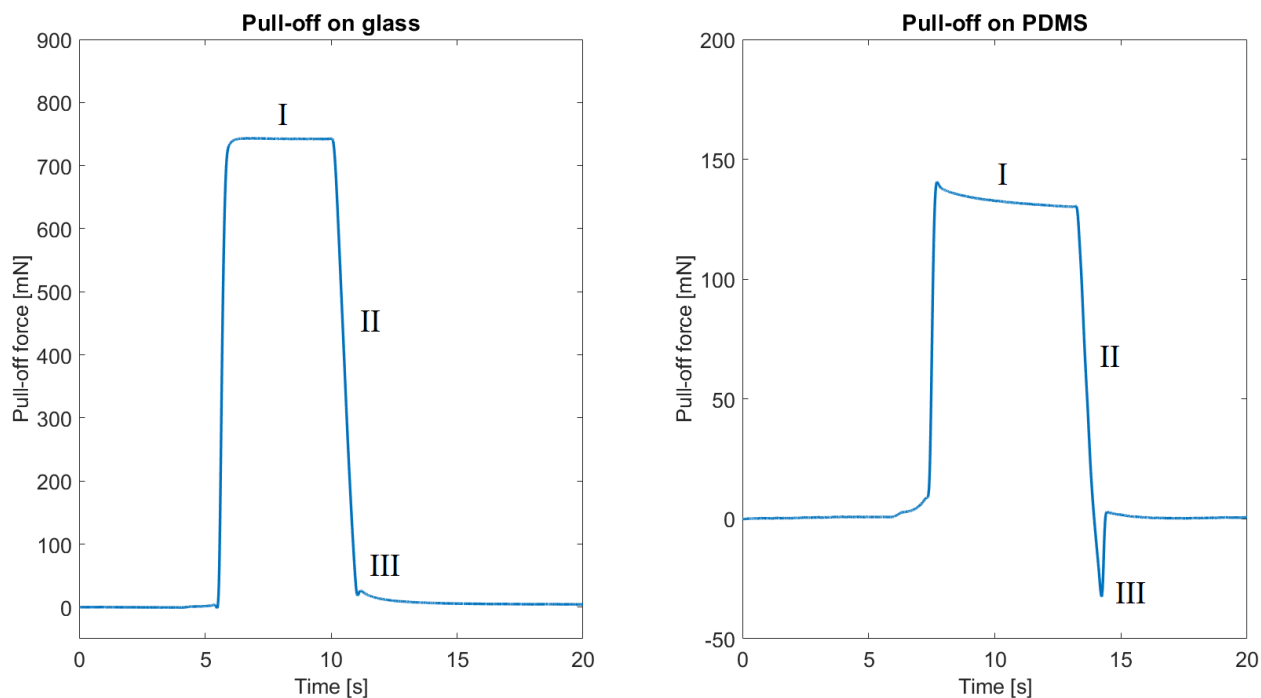


**Figure 7.** Pull-off forces of micropatterned adhesives from glass (left) and PDMS (right) in time. I) The adhesive was positioned in its point of calibrated contact with the substrate. II) The adhesive was moved away at  $100 \mu\text{m/s}$  perpendicular to the substrate. III) The local minimum indicates the point of detachment of the adhesive from the substrate, and is defined as the pull-off force.

The maximum pull-off forces of the four adhesives (with varying pillar diameter and spacing) from glass and PDMS are shown in Figure 8. A strongly significant main effect for substrate stiffness ( $F(1,72) = 24.17$ ,  $p < 0.001$ ) is shown by a two-way ANOVA for adhesive pattern (unpatterned, d40s20, d80s20 and d80s40) and substrate stiffness (580 kPa and 73.6 GPa). The interaction effect between adhesive pattern and substrate stiffness ( $F(3,72) = 4.12$ ,  $p = 0.0094$ ), and the main effect of adhesive pattern ( $F(3,72) = 3.08$ ,  $p = 0.033$ ) are also found to be significant. On glass, post-hoc analysis showed that adhesives with a d80s40-pattern exerted lower pull-off forces compared to unpatterned adhesives ( $p = 0.0298$ ). On PDMS, no significant differences between the pull-off forces of the four types of adhesives are observed. Post-hoc analysis showed that adhesives with a d40s20-pattern and adhesives with a d80s20-pattern generated significantly higher pull-off forces on PDMS-substrates compared to glass-substrates (d40s20-adhesives:  $p = 0.013$ ; d80s20-adhesives:  $p = 0.0011$ ).

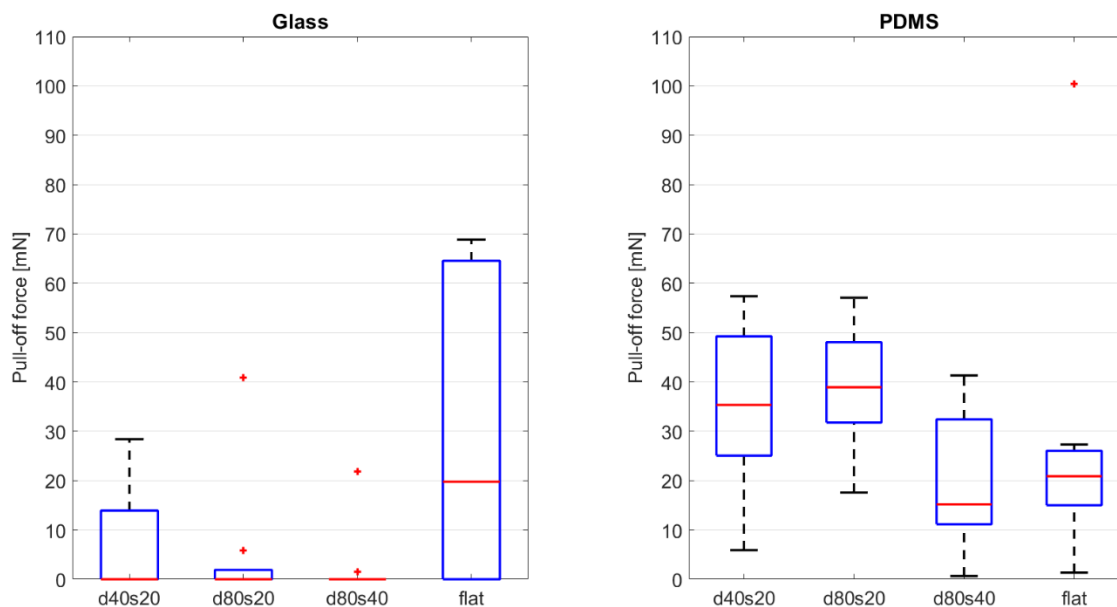


**Figure 8.** Maximum pull-off forces of adhesives with a d40s20-, d80s20-, d80s40-pattern and an unpatterned adhesive on glass (left) and PDMS (right). Ten measurements are conducted per adhesive.

## Friction

Representative force-time plots of friction measurements of micropatterned adhesives on glass and PDMS are shown in Figure 9. The maximum (static) friction force corresponds with the point in time on which the adhesive started sliding on the substrate.

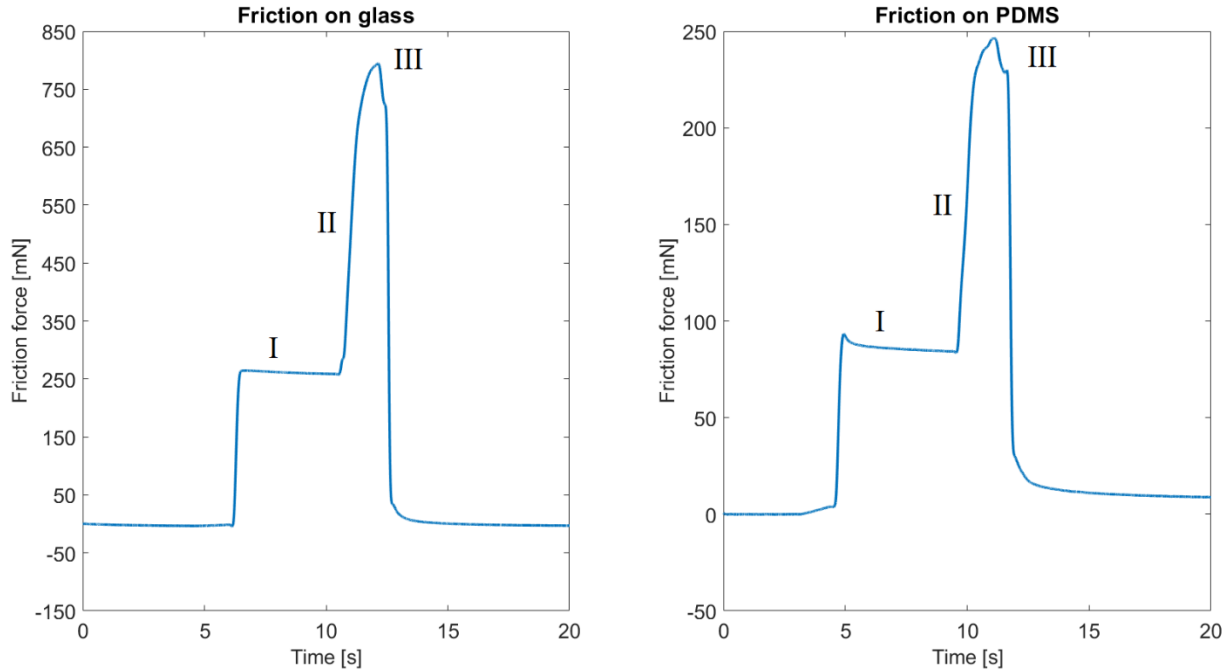


**Figure 9.** Friction forces of micropatterned adhesives on glass (left) and PDMS (right) in time. I) The adhesive was positioned in its point of calibrated contact with the substrate. II) The adhesive was displaced at  $50 \mu\text{m/s}$  in lateral direction on the substrate. The static friction force corresponds with the moment on which the adhesive started sliding on the substrate. III) When the adhesive stopped sliding, it was pulled off from the substrate.

Figure 10 shows the maximum friction forces of the four adhesives on glass and PDMS. A two-way ANOVA for adhesive pattern (unpatterned, d40s20, d80s20 and d80s40) and substrate stiffness (580 kPa and 73.6 GPa) showed strongly significant main differences for adhesive pattern ( $F(3,72) = 20.72$ ,  $p < 0.001$ ), substrate stiffness ( $F(1,72) = 250.16$ ,  $p < 0.001$ ), and their interaction ( $F(3,72) = 16.56$ ,  $p < 0.001$ ). On glass, post-hoc analysis showed that the adhesive with a d40s20-pattern as well as the adhesive with a d80s40-pattern generated strongly significantly higher friction forces compared to the d80s20-adhesive pattern and the unpatterned adhesive (all with  $p < 0.001$ ). On PDMS, no significant statistical differences between the friction forces of the four adhesives were found. Compared to PDMS, all adhesives showed significant higher friction forces on glass ( $p < 0.001$  for the d40s20-pattern, the d80s40-pattern and the unpatterned adhesive;  $p = 0.0055$  for the d80s20-pattern).

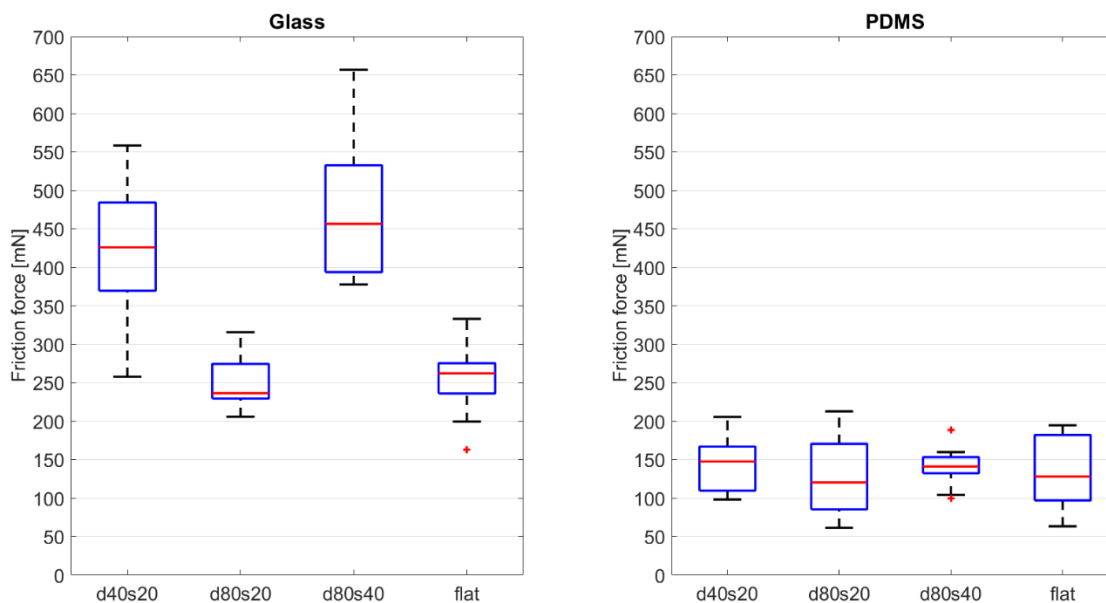


**Figure 10.** Maximum friction forces of adhesives with a d40s20-, d80s20-, d80s40-pattern and an unpatterned adhesive on glass (left) and PDMS (right). Ten measurements are conducted per adhesive.

## DISCUSSION

### Drainage

#### *Flow direction*

As stated in the results-section, the direction of the particle flow varied per experiment. It is likely that the flow direction depends on the location of the adhesive-substrate contact area relative to the top of the substrate. Additionally, the shape and the position of the initial droplet relative to the top of the substrate affects the flow direction upon approach.

Within a measurement, the direction of the flow often changed at several separation distances between adhesive and substrate (see results-section). These separation distances did not necessarily coincide with the critical heights – the separation distances at which the channels begin to play a role in draining the fluid from the interface – as defined by Gupta & Fréchet (Table S2).<sup>45</sup> Apparently, the sudden changes in flow direction are not directly caused by the initiation of drainage through the channels. A possible explanation for the changes in flow direction could be that the coherence of the droplet and the surface tension at the air-water-substrate interface resulted in piling up the fluid at the edge of the substrate. As a consequence, the magnitude of the resisting force at the edge of the substrate – in the opposite direction to the initial flow direction – increased and eventually changed the flow direction. This process happened at a relative slow pace and does not explain abrupt changes in flow direction, though. Trajectories and velocities of independent particles could still be distinguished despite their random flow directions.

At one particular moment, the direction of the flow often suddenly changed before it was decelerated, namely just before the end of the approach phase. This moment coincides with the moment at which the adhesive comes in contact with the substrate. This could explain the sudden change in flow direction.



### *Flow trajectory*

In general it can be said that the pillars acted as obstacles around which the particles were deflected, resulting in the semi-wave pattern (Figure 5). The combination of the straight and semi-wave flow trajectory in the orthogonal flow direction (Figure 5) is probably also the result of the circular pillars on the adhesives. Namely, as the driving force pressed the flow to the side of the channels and since the side of the channels consisted of circular pillars, the counteracting force was constant at point A but faded away as the fluid approached point B. Therefore, the fluid deflected towards point B. After reaching point B, the driving force was the only force that acted upon the fluid, such that the fluid was attracted to the straight path and flowed again through the small gap between the pillars. A full-wave pattern – particles flowing around the pillars – rarely occurred. Apparently, this path is energetically not optimal.

### *Flow velocity*

The plot in Figure 6 gives a few clear insights in the particle velocity during the experiments. First of all, the absolute average velocity of the particles before the point of calibrated contact strongly varies among the repetitions of the same condition. This could be due to the fact that the location of the droplet and the extent to which it is uniformly spread relative to the top of the hemispherical substrate varies per experiment.

Second, there seems to be a time-region with high-velocity particles and a time-region with low-velocity particles, which are separated from each other at ca. 2s before the adhesive reaches the calibrated contact position at  $t = 0$  s. This moment coincides with the moment at which the adhesive touches the substrate. The most probable cause of the decrease in particle velocity is the presence of high hydrodynamic forces at small separation distances between adhesives and substrates, causing the fluid to be squeezed out of the channels.<sup>27,45–50</sup> Because of the decrease of the amount of fluid in the channels, the particle velocity decreased as well. Also, since the calibrated contact position was situated 100  $\mu\text{m}$  below the position where the first pillars touched the substrate, and since the pillar height is ca. 55  $\mu\text{m}$ , some channels were partly blocked. These channels may have acted like a wall by which the particle flow was decelerated. Thirdly, the low wetting ability of the hydrophobic PDMS channel walls and the strong cohesion of the water droplet could also partly explain this result. It can be observed that when the adhesive stopped moving, the particle velocity remained more or less constant. This suggests that that no other (material- or micropattern-related) driving force is present on the interface in both cases.

Finally, it can be observed that the particles have a similar velocity on the glass and the PDMS substrate during the complete time span (Figure 6). This was unexpected, because it was visually observed that the fluid layer thickness was smaller on the glass substrate (due to its more hydrophilic character and thus higher fluid spreadability) than on the PDMS substrate. Moreover, in literature it is argued that softer substrates have better dewetting properties.<sup>22–24</sup> This would have led to a smaller particle velocity on the glass substrate compared to the PDMS substrate. However, from the force-time curves it appeared that the normal forces were much higher in the calibrated contact position (phase I) on glass than on PDMS (Figure 7). This is likely to be due to the fact that PDMS deforms under the normal load of the adhesive, and glass does not because of its higher elastic modulus. Because of the high force on glass, the backing layer of micropatterned adhesives could have been conformed into the channels between the pillars. This would have led to squeezing more fluid through the channels on glass, leading to a higher particle velocity than expected. Therefore, it is possible that the effects of the high wetting capability and the low softness of the glass substrate on the particle velocity have cancelled each other out.

## Pull-off

On the PDMS substrate, no significant effect of adhesive pattern (i.e., theoretical contact area, wall area and aspect ratio) on pull-off forces was observed. This was also found by Van Assenbergh et al. on dry interfaces between PDMS adhesives and soft PVA substrates.<sup>57</sup> They proposed that the low surface energy of PVA resulted in a weak adhesive-substrate contact that eventually led to an insignificant difference between the pull-off forces of micropatterned and unpatterned adhesives. Since the PVA coating on the substrates was obviously damaged in this study, the PDMS substrate had a hydrophobic character. Nevertheless weak adhesive-substrate interactions were present, presumably due to screening of Van der Waals interactions by the water. Namely, Van der Waals forces are one order of magnitude lower in a wet environment compared to a dry environment as a result of the high dielectric constant of water.<sup>58</sup> Li et al. also did pull-off measurements on wet, hydrophobic interfaces and observed higher pull-off forces of unpatterned adhesives compared to micropatterned adhesives.<sup>17</sup> This in contrast to our study, but they applied only 3  $\mu\text{L}$  fluid per experiment such that Van der Waals forces were probably much higher at their interface compared to this study. The generated forces in this study were probably mainly caused by hydrodynamic interactions. Therefore, it seems logical that no significant effect of adhesive pattern on PDMS was found.

On the glass substrate, most of the measurements with the micropatterned adhesives resulted in no pull-off force. This smooth detachment of adhesives from glass was also observed in the force-time curves in Figure 7, because the peak pull-off force (phase III) was often not visible on glass. Also, the slope of the curve during detachment (phase II) was less steep on glass than on PDMS, indicating a faster detachment of the adhesive from glass. Consequently, significant main effects of the substrate stiffness and of the interaction between substrate stiffness and adhesive pattern on pull-off forces were shown. In literature the rule of thumb seems to be that pull-off forces are higher for softer surfaces due to an enlarged contact area and better dewetting properties, which could have explained the different results for micropatterned adhesives on the two substrates.<sup>17,21-24</sup> In this study, however, the particle velocities were similar on both substrates (Figure 6). Also, the pull-off force of unpatterned adhesives was comparable on PDMS and glass. Therefore, the geometrical difference of micropatterned and unpatterned adhesives should also be taken into account.

A possible explanation for the differences in pull-off force from glass and PDMS is the presence of a thinner fluid layer on the glass substrate. Namely, the plot in Figure 6 shows that the particle velocity was similar on glass and PDMS for the d80s20-adhesive. The fluid layer, however, was already thinner on the glass substrate compared to the PDMS substrate at the start of the experiment due to the glass's hydrophilic character. Although pull-off forces generally increase with decreasing fluid volume on the interface of a micropatterned adhesive and a substrate (shown in practice<sup>8,9,16,17,28,30-32</sup> and according to theory<sup>29</sup>), a reversed relation for small fluid volumes is also found in literature on this length scale. Gong et al. and Drotlef et al. observed that pull-off forces can be maximized with fluid volumes in the order of less than a tenth of a microliter.<sup>9,16</sup> This could be due to capillary forces that strongly contribute to the generation of pull-off forces on wet interfaces, and that are maximized at a small separation distance, i.e. when a thin fluid layer is present at the interface.<sup>17</sup> This is supported by Gorb & Gorb, who suggested that the capillary interaction at an interface reduces with a thinner fluid film when the film thickness is already small.<sup>59</sup> Other studies have also suggested or shown that pull-off forces decrease with a decreasing amount of fluid for small fluid volumes.<sup>9,16,33,60,61</sup> Therefore, it is possible that Van der Waals forces could not be generated in this study due to the absence of dry adhesive-substrate contact, and that the fluid layer on the interface was too thin to generate high capillary forces, resulting in low or no pull-off forces on the glass substrate. For interfaces with unpatterned adhesives, the raw data showed that the particle velocity was obviously lower compared to interfaces with micropatterned adhesives. The resulting thicker

fluid layer on interfaces with unpatterned adhesives could explain the comparable pull-off forces of unpatterned adhesives on both substrates.

During the measurements on PDMS and glass, conformation of the substrate to the adhesive did likely not occur, because the elastic modulus of the substrate was higher than the effective elastic modulus of the (micropillars on the) adhesive.<sup>62,63</sup> Therefore, the tips of the pillars can be considered as individual contact points. From the results presented in this paper, it seems that no consistent relation between the aspect ratio and pull-off forces in wet environments on both substrates exists.

## Friction

By comparing the friction data of the two substrates, it is found that the shear forces were significantly higher on glass. In literature, however, friction forces of micropatterned as well as unpatterned adhesives in a wet environment seem to be higher on softer surfaces.<sup>13,20</sup> Literature seems to be more in line with the results in this paper when it comes to the hydrophilicity of the adhesive and the substrate. For example, Drotlef et al. showed that shear forces of hydrophilic, micropatterned adhesives were higher than those of hydrophobic, micropatterned adhesives, which is in accordance with our results.<sup>16</sup> Therefore, it is assumable that the fluid film thickness on the substrates plays a larger role compared to the softness of the substrates. As discussed before, the fluid layer was thinner on glass due to the hydrophilic character of the glass substrate. Since friction forces generally increase with a decreasing fluid volume on the interface of a micropatterned adhesive and a substrate (according to Newton's law of viscosity for friction, and shown in experimental studies<sup>3,20,30,32</sup>), higher shear forces were generated on glass.

On the PDMS substrate, no significant effect of adhesive pattern on friction forces is shown. In literature, it is shown that micropatterned adhesives generated higher shear forces compared to unpatterned adhesives on a hydrophobic substrate in submerged conditions, whereas an opposite trend was shown with a small fluid volume on an interface.<sup>5,11,16</sup> It is possible that the amount of fluid that was present on the interface in our study was equal to the fluid volume that corresponded with the tipping point, which could explain the more or less equal shear forces of the unpatterned and micropatterned adhesives on the PDMS substrate. Moreover, as explained earlier for the pull-off forces on PDMS, the wet conditions, the hydrophobic character of PDMS, and the relatively low normal load on the PDMS substrate could have caused a weak adhesive-substrate contact. This could explain the insignificant differences of the friction forces among the micropatterned and unpatterned adhesives.

On the glass substrate, the d40s20- and d80s40-adhesives generated obviously higher friction forces compared to the other two adhesives. It is remarkable that these two adhesives also have the largest channel area (i.e. the smallest contact area) and the smallest relative wall area among the four adhesives (Table 1). The drainage properties of the adhesives with a d40s20- and d80s40-pattern were likely best, resulting in a smaller fluid film thickness, and thus higher shear forces. The results are comparable with the results of Li et al., Iturri et al. and Drotlef et al., who showed that micropatterned adhesives generated higher shear forces compared to unpatterned adhesives on hydrophilic interfaces.<sup>5,11,16</sup>

On glass and on PDMS, the d40s20-adhesive – the adhesive with the largest aspect ratio – generated higher or similar friction forces compared to the other adhesives, which is in contrast with the outcomes of previous work. Namely, Drotlef et al. and Iturri et al. have shown that an increasing aspect ratio of pillars made of PDMS causes pillars to be more deformable, which leads to pillar clustering, and consequently reduces the contact area and thus the friction force of a micropatterned adhesive on a substrate.<sup>11,16</sup> In this work, the d40s20-adhesive had a larger aspect ratio compared to the tallest pillars in the studies of Iturri et al. and Drotlef et al..<sup>11,16</sup> As expected, it was observed that buckling of pillars did occur during shear movement. The frequency and the extent to which the pillars buckled was higher on

d40s20-adhesives compared to the d80s20- and d80s40-adhesives. As discussed before for pull-off, the tips of the pillars can be considered as individual contact points. Therefore, it is assumable that the relatively high preload in this study – compared to the preload of 1 mN in the studies of Iturri et al. and Drotlef et al. – have pressed buckled pillars onto the substrate, such that pillars did not have a chance to form clusters and the contact area did not decrease.

A less significant main effect of adhesive pattern was found for pull-off forces compared to shear forces. This could be related to the suspect that an optimum fluid volume exists to generate maximum pull-off forces, which does not exist for friction forces. Therefore, fast drainage of fluid from the interface (by which channels on an interface could come into play) is likely not desirable to generate the highest pull-off forces, but it could be to generate the highest shear forces. This hypothesis is supported by literature. Varenberg & Gorb, Li et al. and Ko et al. showed that large spacing ratios (i.e., large channel areas) increase shear forces.<sup>3,5,25</sup> Moreover, the decrease in friction due to pillar clustering is previously explained by a decrease in contact area, but the channel area and/or volume decreases as well and could therefore also play a role. It is also shown that smaller channel width-to-length ratios, i.e., smaller spacing ratios or larger pillar area ratios – that reduce the channel area – increase pull-off forces.<sup>7,26–28</sup>

## Limitations

### *Experimental setup*

As substantiated in the paper, the effect of the differences in hydrophilicity and preload in the calibrated contact position among the substrates probably dominates over any other effects of the difference in softness of the substrates on the drainage, pull-off, and friction data. The results that are presented give rise to the question whether a lower preload always increases pull-off forces and decreases friction forces in wet conditions, and whether these results only hold in submerged conditions or also in small fluid volumes. These are interesting topics for future work.

To investigate the effect of softness of the substrates on pull-off and friction *during* pull-off and sliding movements, the effect of softness of the substrates should be minimized *prior* to the experiment. Hemispherical substrates were used in this work, because pull-off forces have been shown to be independent of the misalignment angle between an adhesive and a hemispherical substrate on dry interfaces.<sup>64</sup> The dynamic contact area of hemispherical substrates during detachment as reported by Kamperman et al. and the misaligned pillars in the periphery of hemispherical substrates as reported by Kroner et al. were less important in this study, because the topic of interest of this study was the maximum adhesive and friction force.<sup>64,65</sup> However, a high preload is required to maximize the adhesive-substrate contact area on hemispherical substrates, but also induces a difference in preload on substrates of different stiffness degrees. A plate-to-plate configuration would eliminate the need for a high preload in the calibrated contact position, because the contact area is then already maximized upon contact with a flat substrate. It should be kept into account that alignment issues should be carefully avoided in a plate-to-plate configuration by using a sound alignment system based on optical, force and/or gravitational feedback. Another way of making sure that the same preload is applied on substrates with different stiffness degrees is to use force feedback to define the calibrated contact position, instead of defining this position based on a pre-defined displacement value, as was done in this work. The adhesive-substrate contact area of the glass and PDMS substrate will not be comparable when force feedback is used to define the calibrated contact position.

Alignment issues in the setups in this work have probably played an important role during the generation of the results. In the drainage setup, the middle of the adhesive is located above the top of the hemispherical substrate by real-time monitoring of the adhesive-substrate contact area via the

microscope (i.e., from the top of the setup). Also, visual inspection of the position of the adhesive relative to the substrate from both of the sides of the setup was executed by eye. Besides, the shape and location of the initial droplet relative to the top of the substrate varied per experiment, because no additional alignment instruments were used during fluid deposition. In the setup for the pull-off and friction experiments, adhesive-substrate alignment was monitored via a magnifying camera from the side, which resulted in more accurate adhesive-substrate alignment compared to the drainage setup. As discussed before, small misalignments of the adhesive-substrate contact and the location of the fluid on the substrate could have caused variations in drainage direction and flow velocity, and possibly in the pull-off and friction forces. Therefore, it is recommended to use more advanced alignment techniques for the relative adhesive-substrate and fluid-substrate positions in future work.

Although the substrates were coated, the contact angle of the fluid differed among the glass and the PDMS substrate. The coating was probably degraded during the cleaning procedure of the experiments. To eliminate the effect of hydrophilicity in future work, another coating technique should be used or another cleaning procedure should be applied.

During the drainage experiments, particles were tracked. To what extent particle behavior is representative for fluid flow depends on the buoyancy of the particles and the duration of the experiments amongst others. The density of the polystyrene latex beads (1.005 kg/L) is a bit larger than that of the rest of the suspension (0.998 kg/L), i.e., the particles are not neutrally buoyant. However, since this difference is small, the particles have a velocity in the horizontal plane and the time span in which the particles become visible until they reach a steady velocity only lasts for a few seconds, the vertical displacement of the particles during the experiment is considered to be negligible. Therefore, the particles that were tracked are considered to represent the fluid flow correctly.

It would have been better to express the drainage capability of an interface in a different way. The drainage velocity was captured in one horizontal plane at a time in this study, but differences in drained fluid *volume* from different interfaces could not be analyzed in this way. Besides, the water level in the channels as a result of the pre-wetting procedure and during the experiments could not be validated. Therefore, an alternative would be to express the drainage results in volumetric flow rate instead of particle velocity, by either modelling or measuring the flow in the normal plane.

#### *Data analysis of the drainage results*

Improvements on the method for data analysis can be implemented in the pre-processing and the post-processing stage. In the pre-processing stage, the current method detects (part of) the pixels of the perimeter of an in-focus particle. The number of detected pixels per in-focus particle varies, because it is related to the grey value and thus the extent to which a particle is in focus. Since the average velocity of the pixels is calculated during analysis, the results are biased: it has become a weighted average of the velocity of the detected *pixels*, instead of an average of all in-focus *particles*. Therefore, it is recommended to implement a method to detect particles as one object.

In the post-processing stage, the current analysis could be extended. First, more plots could be generated to allow for an elaboration of the analysis of the within and between experiment conditions characteristics. For example, when the particle velocity at the interfaces with unpatterned and micropatterned adhesives in time can be compared, the hypothesis of the existence of three fluid flow regimes while peeling or moving a micropatterned surface with cylindrical posts from or normal to a flooded substrate could be validated.<sup>45,47</sup> By plotting the particle velocity against separation distance, it could also be investigated whether the moments at which changes in particle velocity take place coincide with the critical heights as defined by Gupta & Fréchet and Dhong & Fréchet.<sup>45,47</sup> Moreover, the particle velocity could be related to the size of the wetted *channel* area, and the size (i.e., the extent to which the adhesive was pressed onto the substrate) and the relative location of the *contact* area of the

adhesive on the substrate. These factors could possibly explain abrupt changes in flow direction, trajectory and velocity, as well as deviations of the particle velocity among the repetitions of experiment conditions. Images of the contact area and the size of the wetted channel area per experiment can be used for this purpose. Next to this, it would be useful to generate statistical information about the experiments to assess the repeatability of the experiments.

## CONCLUSIONS

In this work, the fluid flow behavior on wet adhesive-substrate interfaces was captured on three focal planes, and related to the pull-off and friction forces of the adhesive on the substrate. It has been shown that changes in flow direction during approach of a micropatterned adhesive are probably not directly related to the initiation of drainage through its channels; the heights at which the latter is probable to happen being suggested in previous studies. Besides, two typical flow trajectories are identified: a straight flow path and a semi-wave flow path. It was observed that the flow velocity was lower when the flow path was wider. Moreover, two velocity regions related to the separation distance between the two surfaces could be distinguished: a high-velocity region before adhesive-substrate contact was established, and a low-velocity region after the point of contact. A clear difference in flow velocity between the two substrates did not exist, which could be due to the effects of the stiffness and the wetting capability of the substrates cancelling each other out. The results suggest that a larger channel area on the micropatterned adhesives could increase shear forces, but that a large channel area is not necessarily desirable to generate the highest pull-off forces. This could be related to the possible existence of an optimum fluid volume for which pull-off forces are maximized, which does not exist for shear forces.

## ASSOCIATED CONTENT

### Supporting Information

The following files are available free of charge:

Drainage measurements: detailed setup and design choices, drawings of the setup, scripts for data analysis, visual observations from the raw data per experiment; pull-off and friction measurements: details of the setup, drawing of the setup, scripts for data analysis (PDF)

## AUTHOR INFORMATION

### Corresponding Author

\* E-mail: [B.A.HaitsmaMulier@student.tudelft.nl](mailto:B.A.HaitsmaMulier@student.tudelft.nl)

### Notes

The authors declare no competing financial interest.

## ACKNOWLEDGMENTS

This research is supported by the Netherlands Organization for Scientific Research (NWO) Domain Applied and Engineering Sciences (TTW), (Open Technology Program, project 13353 “Secure and gentle grip of delicate biological tissues”). We acknowledge Henny van der Ster and David Jager from the Electronic and Mechanical Support Division (DEMO) of the Delft University of Technology for manufacturing the setup of the drainage measurements and the substrate holders for the setup of the pull-off and friction measurements. We also acknowledge Patrick van Holst, Gideon Emmaneel and Alex van den Bogaard from the Precision and Microsystems Engineering (PME) support division of the Delft University of Technology for giving us access to the Keyence microscope and providing us with the necessary instruction and information. We also thank Kai Zhang for fabricating the PDMS substrate, and Daniel Yi for manufacturing the silicon wafer for the fabrication of the adhesives.

## REFERENCES

- (1) Barnes, J.; Smith, J.; Oines, C.; Mundl, R. Bionics and Wet Grip. *Tire Technol. Int.* **2002**, *dec*, 56–60.
- (2) Chen, D.; Zhang, Y.; Long, G.; Liu, W.; Li, X.; Sun, Y.; Chang, Z. An Optimal Wet Friction Plate Inspired by Biological Surface Patterns. *J. Bionic Eng.* **2018**, *15* (5), 872–882. <https://doi.org/10.1007/s42235-018-0074-0>.
- (3) Varenberg, M.; Gorb, S. N. Hexagonal Surface Micropattern for Dry and Wet Friction. *Adv. Mater.* **2009**, *21* (4), 483–486. <https://doi.org/10.1002/adma.200802734>.
- (4) Rao, P.; Sun, T. L.; Chen, L.; Takahashi, R.; Shinohara, G.; Guo, H.; King, D. R.; Kurokawa, T.; Gong, J. P. Tough Hydrogels with Fast, Strong, and Reversible Underwater Adhesion Based on a Multiscale Design. *Adv. Mater.* **2018**, *30* (32), 1801884. <https://doi.org/10.1002/adma.201801884>.
- (5) Li, M.; Huang, W.; Wang, X. Bioinspired, Peg-Studded Hexagonal Patterns for Wetting and Friction. *Biointerphases* **2015**, *10* (3), 031008. <https://doi.org/10.1116/1.4930176>.
- (6) Persson, B. N. J. Biological Adhesion for Locomotion: Basic Principles. *J. Adhes. Sci. Technol.* **2007**, *21* (12–13), 1145–1173. <https://doi.org/https://doi.org/10.1163/156856107782328335>.
- (7) Endlein, T.; Barnes, W. J. P.; Samuel, D. S.; Crawford, N. a.; Biaw, A. B.; Grafe, U. Sticking under Wet Conditions: The Remarkable Attachment Abilities of the Torrent Frog, *Staurois Guttatus*. *PLoS One* **2013**, *8* (9), e73810. <https://doi.org/10.1371/journal.pone.0073810>.
- (8) Federle, W.; Barnes, W. J. P.; Baumgartner, W.; Drechsler, P.; Smith, J. M. Wet but Not Slippery: Boundary Friction in Tree Frog Adhesive Toe Pads. *J. R. Soc. Interface* **2006**, *3* (10), 689–697. <https://doi.org/10.1098/rsif.2006.0135>.
- (9) Gong, L.; Yu, H.; Wu, X.; Wang, X. Wet-Adhesion Properties of Microstructured Surfaces Inspired by Newt Footpads. *Smart Mater. Struct.* **2018**, *27* (11), 114001. <https://doi.org/10.1088/1361-665X/aad6d2>.
- (10) Hanna, G.; Barnes, W. J. P. Adhesion and Detachment of the Toe Pads of Tree Frogs. *J. Exp. Biol.* **1991**, *155* (1), 103–125.
- (11) Iturri, J.; Xue, L.; Kappl, M.; García-Fernández, L.; Barnes, W. J. P.; Butt, H.-J.; del Campo, A. Torrent Frog-Inspired Adhesives: Attachment to Flooded Surfaces. *Adv. Funct. Mater.* **2015**, *25* (10), 1499–1505. <https://doi.org/10.1002/adfm.201403751>.
- (12) Huang, W.; Wang, X. Biomimetic Design of Elastomer Surface Pattern for Friction Control under Wet Conditions. *Bioinspiration and Biomimetics* **2013**, *8* (4), 046001. <https://doi.org/10.1088/1748-3182/8/4/046001>.
- (13) Kappl, M.; Kaveh, F.; Barnes, W. J. P. Nanoscale Friction and Adhesion of Tree Frog Toe Pads.

- Bioinspiration and Biomimetics* **2016**, *11* (3), 035003. <https://doi.org/10.1088/1748-3190/11/3/035003>.
- (14) Tsipenyuk, A.; Varenberg, M. Use of Biomimetic Hexagonal Surface Texture in Friction against Lubricated Skin. *J. R. Soc. Interface* **2014**, *11* (94), 20140113. <https://doi.org/10.1098/rsif.2014.0113>.
  - (15) Langowski, J. K. A.; Dodou, D.; Kamperman, M.; van Leeuwen, J. L. Tree Frog Attachment: Mechanisms, Challenges, and Perspectives. *Front. Zool.* **2018**, *15* (1), 1–21. <https://doi.org/10.1186/s12983-018-0273-x>.
  - (16) Drotlef, D. M.; Stepien, L.; Kappl, M.; Barnes, W. J. P.; Butt, H. J.; Del Campo, A. Insights into the Adhesive Mechanisms of Tree Frogs Using Artificial Mimics. *Adv. Funct. Mater.* **2013**, *23* (9), 1137–1146. <https://doi.org/10.1002/adfm.201202024>.
  - (17) Li, M.; Xie, J.; Dai, Q.; Huang, W.; Wang, X. Effect of Wetting Case and Softness on Adhesion of Bioinspired Micropatterned Surfaces. *J. Mech. Behav. Biomed. Mater.* **2018**, *78* (June 2017), 266–272. <https://doi.org/10.1016/j.jmbbm.2017.11.036>.
  - (18) Barnes, W. J. P. Adhesion in Wet Environments: Frogs. *Encyclopedia of Nanotechnology*; **2012**; pp 70–83.
  - (19) Shin, D., & Meredith, J. C. Influence of Topography on Adhesion and Bioadhesion. In *Advances in Polymer Science*; Springer: Berlin, Heidelberg, **2017**; pp 1–32. [https://doi.org/https://doi.org/10.1007/12\\_2017\\_40](https://doi.org/https://doi.org/10.1007/12_2017_40).
  - (20) Mizushima, K.; Nishimura, T.; Suzuki, Y.; Tsuji, T.; Watanabe, T. Surface Texture of Deformable Robotic Fingertips for a Stable Grasp under Both Dry and Wet Conditions. *IEEE Robot. Autom. Lett.* **2017**, *2* (4), 2048–2055. <https://doi.org/10.1109/LRA.2017.2717082>.
  - (21) Kaveh, F.; Ally, J.; Kappl, M.; Butt, H. J. Hydrodynamic Force between a Sphere and a Soft, Elastic Surface. *Langmuir* **2014**, *30* (39), 11619–11624. <https://doi.org/10.1021/la502328u>.
  - (22) Brochard-Wyart, F.; Buguin, A., Martin, P., Martin, A., & Sandre, O. Adhesion of Soft Objects on Wet Substrates. *J. Phys. Condens. Matter* **2000**, *12* (8A), A239–A244.
  - (23) Martin, P., Silberzan, P., & Brochard-Wyart, F. Sessile Droplets at a Solid/Elastomer Interface. *Langmuir* **1997**, *13* (18), 4910–4914.
  - (24) Martin, P., & Brochard-Wyart, F. Dewetting at Soft Interfaces. *Phys. Rev. Lett.* **1998**, *80* (15), 3296.
  - (25) Ko, H.; Seong, M.; Jeong, H. E. A Micropatterned Elastomeric Surface with Enhanced Frictional Properties under Wet Conditions and Its Application. *Soft Matter* **2017**, *13* (45), 8419–8425. <https://doi.org/10.1039/c7sm01493g>.
  - (26) Roshan, R.; Jayne, D. G.; Liskiewicz, T.; Taylor, G. W.; Gaskell, P. H.; Chen, L.; Montellano-Lopez, A.; Morina, A.; Neville, A. Effect of Tribological Factors on Wet Adhesion of a Microstructured Surface to Peritoneal Tissue. *Acta Biomater.* **2011**, *7* (11), 4007–4017. <https://doi.org/10.1016/j.actbio.2011.06.045>.
  - (27) Xie, J.; Li, M.; Dai, Q.; Huang, W.; Wang, X. Key Parameters of Biomimetic Patterned Surface for Wet Adhesion. *Int. J. Adhes. Adhes.* **2018**, *82* (January), 72–78. <https://doi.org/10.1016/j.ijadhadh.2018.01.004>.
  - (28) Cheung, E.; Sitti, M. Adhesion of Biologically Inspired Oil-Coated Polymer Micropillars. *J. Adhes. Sci. Technol.* **2008**, *22* (5–6), 569–589. <https://doi.org/10.1163/156856108X295545>.
  - (29) Barnes, J. Tree Frogs and Tire Technology. *Tire Technol. Int.* **1999**, No. February, 42–47.
  - (30) Drechsler, P.; Federle, W. Biomechanics of Smooth Adhesive Pads in Insects: Influence of Tarsal Secretion on Attachment Performance. *J. Comp. Physiol. A Neuroethol. Sensory, Neural, Behav. Physiol.* **2006**, *192* (11), 1213–1222. <https://doi.org/10.1007/s00359-006-0150-5>.
  - (31) Bohn, H. F.; Federle, W. Insect Aquaplaning: Nepenthes Pitcher Plants Capture Prey with the Peristome, a Fully Wettable Water-Lubricated Anisotropic Surface. *Proc. Natl. Acad. Sci. U. S. A.* **2004**, *101* (39), 14138–14143. <https://doi.org/10.1073/pnas.0405885101>.



- (32) Bullock, J. M. R.; Drechsler, P.; Federle, W. Comparison of Smooth and Hairy Attachment Pads in Insects: Friction, Adhesion and Mechanisms for Direction-Dependence. *J. Exp. Biol.* **2008**, *211* (20), 3333–3343. <https://doi.org/10.1242/jeb.020941>.
- (33) Kovalev, A. E.; Varenberg, M.; Gorb, S. N. Wet versus Dry Adhesion of Biomimetic Mushroom-Shaped Microstructures. *Soft Matter* **2012**, *8*, 7560–7566. <https://doi.org/10.1039/c2sm25431j>.
- (34) Varenberg, M.; Gorb, S. A Beetle-Inspired Solution for Underwater Adhesion. *J. R. Soc. Interface* **2007**, *5* (20), 383–385. <https://doi.org/10.1098/rsif.2007.1171>.
- (35) Edwards, J. S., & Tarkanian, M. The Adhesive Pads of Heteroptera: A Re-examination. *Proc. R. Entomol. Soc. London. Ser. A, Gen. Entomol.* **1970**, *45* (1–3), 1–5.
- (36) Dixon, A. F. G.; Croghan, P. C.; Gowing, R. P. The Mechanism by Which Aphids Adhere to Smooth Surfaces. *J. Exp. Biol.* **1990**, *152*, 243–253.
- (37) Defante, A. P.; Burai, T. N.; Becker, M. L.; Dhinojwala, A. Consequences of Water between Two Hydrophobic Surfaces on Adhesion and Wetting. *Langmuir* **2015**, *31* (8), 2398–2406. <https://doi.org/10.1021/la504564w>.
- (38) Bradley, L. C.; Bade, N. D.; Mariani, L. M.; Turner, K. T.; Lee, D.; Stebe, K. J. Rough Adhesive Hydrogels (RAd Gels) for Underwater Adhesion. *ACS Appl. Mater. Interfaces* **2017**, *9* (33), 27409–27413. <https://doi.org/10.1021/acsami.7b08916>.
- (39) Butt, H. J.; Barnes, W. J. P.; Del Campo, A.; Kappl, M.; Schönfeld, F. Capillary Forces between Soft, Elastic Spheres. *Soft Matter* **2010**, *6* (23), 5930–5936. <https://doi.org/10.1039/c0sm00455c>.
- (40) He, B.; Wang, Z.; Li, M.; Wang, K.; Shen, R.; Hu, S. Wet Adhesion Inspired Bionic Climbing Robot. *IEEE/ASME Trans. Mechatronics* **2014**, *19* (1), 312–320. <https://doi.org/10.1109/TMECH.2012.2234473>.
- (41) Chen, H.; Zhang, L.; Zhang, D.; Zhang, P.; Han, Z. Bioinspired Surface for Surgical Graspers Based on the Strong Wet Friction of Tree Frog Toe Pads. *ACS Appl. Mater. Interfaces* **2015**, *7* (25), 13987–13995. <https://doi.org/10.1021/acsami.5b03039>.
- (42) Arzt, E.; Gorb, S.; Spolenak, R. From Micro to Nano Contacts in Biological Attachment Devices. *Proc. Natl. Acad. Sci. U. S. A.* **2003**, *100* (19), 10603–10606. <https://doi.org/10.1073/pnas.1534701100>.
- (43) Dhong, C. Peeling Structured Surfaces in Viscous Environments: The Role of Deformation and Drainage Channels, Johns Hopkins University, **2016**.
- (44) Persson, B. N. J. Wet Adhesion with Application to Tree Frog Adhesive Toe Pads and Tires. *J. Phys. Condens. Matter* **2007**, *19* (37), 376110. <https://doi.org/10.1088/0953-8984/19/37/376110>.
- (45) Gupta, R.; Fréchet, J. Measurement and Scaling of Hydrodynamic Interactions in the Presence of Draining Channels. *Langmuir* **2012**, *28* (41), 14703–14712. <https://doi.org/10.1021/la303508x>.
- (46) Maali, A.; Pan, Y.; Bhushan, B.; Charlaix, E. Hydrodynamic Drag-Force Measurement and Slip Length on Microstructured Surfaces. *Phys. Rev. E - Stat. Nonlinear, Soft Matter Phys.* **2012**, *85* (6), 1–5. <https://doi.org/10.1103/PhysRevE.85.066310>.
- (47) Dhong, C.; Fréchet, J. Coupled Effects of Applied Load and Surface Structure on the Viscous Forces during Peeling. *Soft Matter* **2015**, *11* (10), 1901–1910. <https://doi.org/10.1039/c4sm02616k>.
- (48) Guriyanova, S.; Semin, B.; Rodrigues, T. S.; Butt, H. J.; Bonaccorso, E. Hydrodynamic Drainage Force in a Highly Confined Geometry: Role of Surface Roughness on Different Length Scales. *Microfluid. Nanofluidics* **2010**, *8* (5), 653–663. <https://doi.org/10.1007/s10404-009-0498-2>.
- (49) Pilkington, G. A.; Gupta, R.; Fréchet, J. Scaling Hydrodynamic Boundary Conditions of Microstructured Surfaces in the Thin Channel Limit. *Langmuir* **2016**, *32* (10), 2360–2368. <https://doi.org/10.1021/acs.langmuir.5b04134>.
- (50) Lorenz, B.; Persson, B. N. J. Fluid Squeeze-out between Rough Surfaces: Comparison of Theory with Experiment. *J. Phys. Condens. Matter* **2011**, *23* (35). <https://doi.org/10.1088/0953-8984/23/35/355005>.

- (51) Park, J. Y.; Yoo, S. J.; Lee, E. J.; Lee, D. H.; Kim, J. Y.; Lee, S. H. Increased Poly(Dimethylsiloxane) Stiffness Improves Viability and Morphology of Mouse Fibroblast Cells. *Biochip J.* **2010**, *4* (3), 230–236. <https://doi.org/10.1007/s13206-010-4311-9>.
- (52) Trantidou, T.; Elani, Y.; Parsons, E.; Ces, O. Hydrophilic Surface Modification of Pdms for Droplet Microfluidics Using a Simple, Quick, and Robust Method via Pva Deposition. *Microsystems Nanoeng.* **2017**, *3*, 16091. <https://doi.org/10.1038/micronano.2016.91>.
- (53) Thorlabs. 1" (25 mm) Travel Motorized Actuators. [https://www.thorlabs.com/newgrouppage9.cfm?objectgroup\\_id=1883&pn=Z825B](https://www.thorlabs.com/newgrouppage9.cfm?objectgroup_id=1883&pn=Z825B) (accessed Nov 20, 2019).
- (54) Bandicam. Bandicam Screen Recorder. [www.bandicam.com](http://www.bandicam.com) (accessed Aug 24, 2019).
- (55) The MathWorks, I. MATLAB. Natick, Massachusetts, United States.
- (56) Thielicke, W. and Stamhuis, E. J. PIVlab - Time-Resolved Digital Particle Image Velocimetry Tool for MATLAB. **2014**. <https://doi.org/http://dx.doi.org/10.6084/m9.figshare.1092508>.
- (57) Assenbergh, P. van; Fokker, M.; Langowski, J.; van Esch, J.; Kamperman, M.; Dodou, D. Pull-off and Friction Forces of Micropatterned Elastomers on Soft Substrates: The Effects of Pattern Length Scale and Stiffness. *Beilstein J. Nanotechnol.* **2019**, *10* (1), 79–94. <https://doi.org/10.3762/bjnano.10.8>.
- (58) Butt, H. J., Graf, K., & Kappl, M. *Physics and Chemistry of Interfaces*; John Wiley & Sons, **2013**.
- (59) Gorb, E. V.; Gorb, S. N. Attachment Ability of the Beetle *Chrysolina Fastuosa* on Various Plant Surfaces. *Entomol. Exp. Appl.* **2002**, *105* (1), 13–28. <https://doi.org/10.1023/A:1021777517981>.
- (60) Kovalev, A. E.; Filippov, A. E.; Gorb, S. N. Insect Wet Steps: Loss of Fluid from Insect Feet Adhering to a Substrate. *J. R. Soc. Interface* **2013**, *10* (78). <https://doi.org/10.1098/rsif.2012.0639>.
- (61) Dirks, J. H.; Federle, W. Mechanisms of Fluid Production in Smooth Adhesive Pads of Insects. *J. R. Soc. Interface* **2011**, *8* (60), 952–960. <https://doi.org/10.1098/rsif.2010.0575>.
- (62) Kaiser, J. S.; Kamperman, M.; De Souza, E. J.; Schick, B.; Arzt, E. Adhesion of Biocompatible and Biodegradable Micropatterned Surfaces. *Int. J. Artif. Organs* **2011**, *34* (2), 180–184. <https://doi.org/10.5301/IJAO.2011.6393>.
- (63) Kern, M. D.; Long, R.; Rentschler, M. E. A Representative Volume Element Model for the Adhesion between a Micro-Pillared Surface and a Compliant Substrate. *Mech. Mater.* **2018**, *119* (August 2017), 65–73. <https://doi.org/10.1016/j.mechmat.2018.01.004>.
- (64) Kroner, E.; Paretkar, D. R.; McMeeking, R. M.; Arzt, E. Adhesion of Flat and Structured PDMS Samples to Spherical and Flat Probes: A Comparative Study. *J. Adhes.* **2011**, *87* (5), 447–465. <https://doi.org/10.1080/00218464.2011.575317>.
- (65) Kamperman, M.; Kroner, E.; Del Campo, A.; McMeeking, R. M.; Arzt, E. Functional Adhesive Surfaces with “Gecko” Effect: The Concept of Contact Splitting. *Adv. Eng. Mater.* **2010**, *12* (5), 335–348. <https://doi.org/10.1002/adem.201000104>.

## Supporting information

# Grip on wet interfaces: an experimental study on the role of drainage

*Babette Haitsma Mulier\*, Peter van Assenbergh, Dimitra Dodou*

Biomechanical Engineering Department, Delft University of Technology, Mekelweg 2, 2628 CD Delft,  
The Netherlands

\* Corresponding author: [B.A.HaitsmaMulier@student.tudelft.nl](mailto:B.A.HaitsmaMulier@student.tudelft.nl)

## S.1 DRAINAGE

### S.1.1 Detailed setup & design choices

A homemade, levelled setup is attached to the microscopic table, as shown in Figure S1. The aluminum base of this setup (5) contains a hole to allow for underexposure of the setup. The light source (7) is located underneath the glass slide in the microscopic table (6) and provides full-ring illumination. In a milled compartment on top of the base, a glass slide is placed such that it bridges the hole. The substrates (4) are fixed to the middle of the glass slide. The glass slide fits exactly in the compartment, such that its movement in the horizontal plane is restricted. To restrict the movement of the glass slide in the normal direction as well, the glass slide is taped to the base. This also allows to switch easily between the substrates.

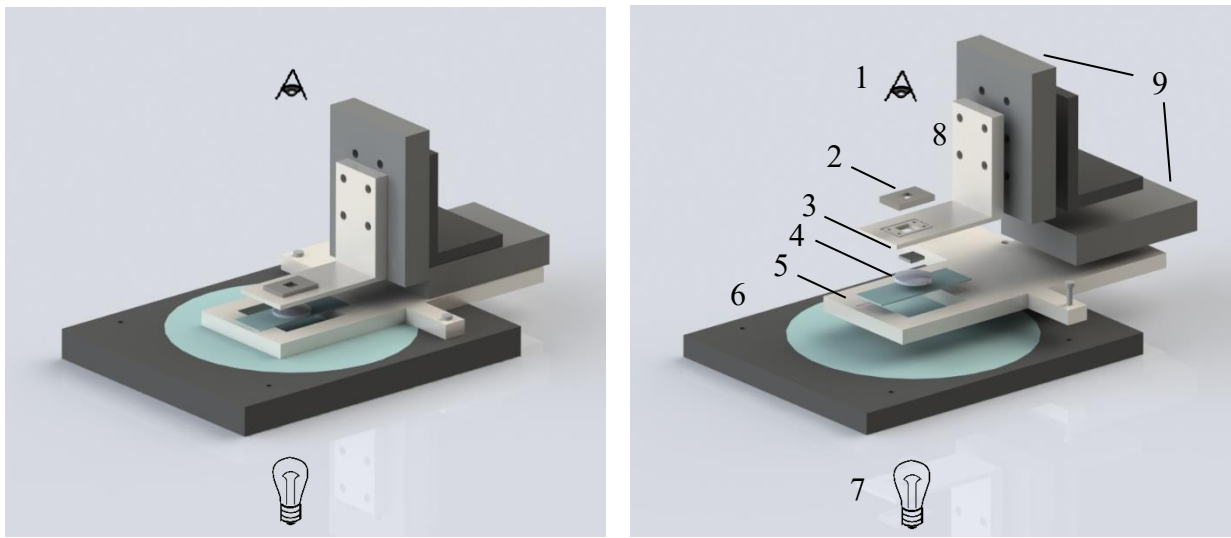


**Figure S1.** Schematic of the setup for the drainage measurements (left) and its exploded view (right). An adhesive (3) is placed in a hole in the cantilever (8) and is locked by a lid (2) in normal direction. The adhesive is positioned exactly above a hemispherical substrate (4) that is placed on a glass slide in an aluminum holder (5), which is mounted to the microscopic table (6). The setup is illuminated from below (7) and viewed from above (1). Two linked, linear translation stages (9) provide normal and lateral movement of the cantilever.

The cantilever (8) contained magnets to which a steel lid (2) attaches to lock the adhesive (3) in the normal direction. A square window is manufactured in the lid, so that the light source can shine through it and the view of the microscope (1) is not blocked. The lid is aligned with the adhesive by means of a gutter in the cantilever. The particle solution is deposited on top of the substrate surface. Therefore, drainage starts upon contact of the adhesive with the fluid. To avoid that the fluid is attracted to the cantilever during the experiment due to surface tension phenomena, Scotch Magic Tape is applied to the bottom of the arm. Also, a compartment is milled at its bottom for this purpose. The resulting distance between the adhesive's pillar tips and the bottom of the arm was 1.2 mm.

The translation stage (9) that provided movement of the cantilever in lateral direction is directly screwed to the aluminum base. The translation stage providing movement in normal direction is connected perpendicular to the other stage via an L-shaped link. The cantilever is connected to the vertical stage.

The theoretical deflection of a solid aluminum beam with the same dimensions as the customized cantilever is 2.2  $\mu\text{m}$  (4% of the pillar height). The deflection (which would have been larger due to the hole, gutter and compartment) is minimized by applying reinforcement with a thickness of 10 mm in the corner of the L-shape of the beam.

### S.1.2 Drawings

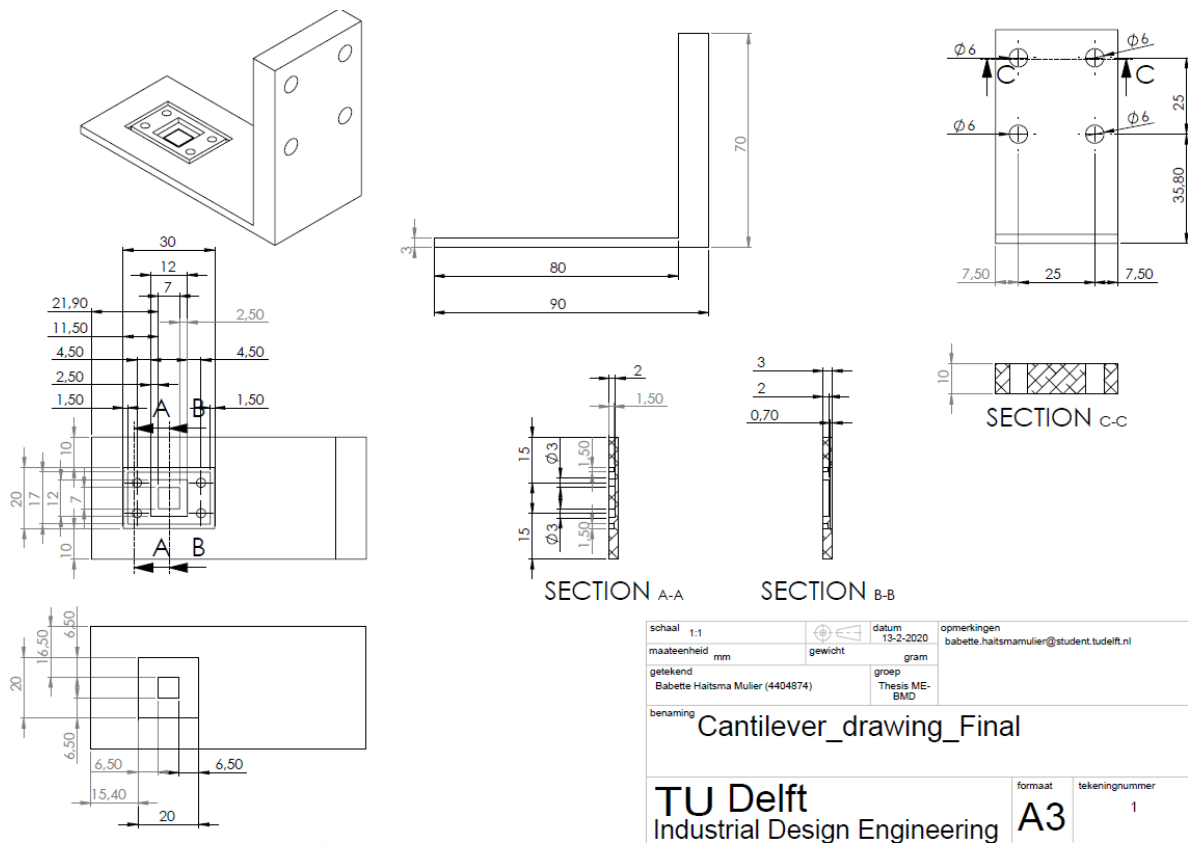


**Figure S2.** Drawing of the cantilever. The reinforcement in the corner of the L-shape of the cantilever is not depicted in this drawing.

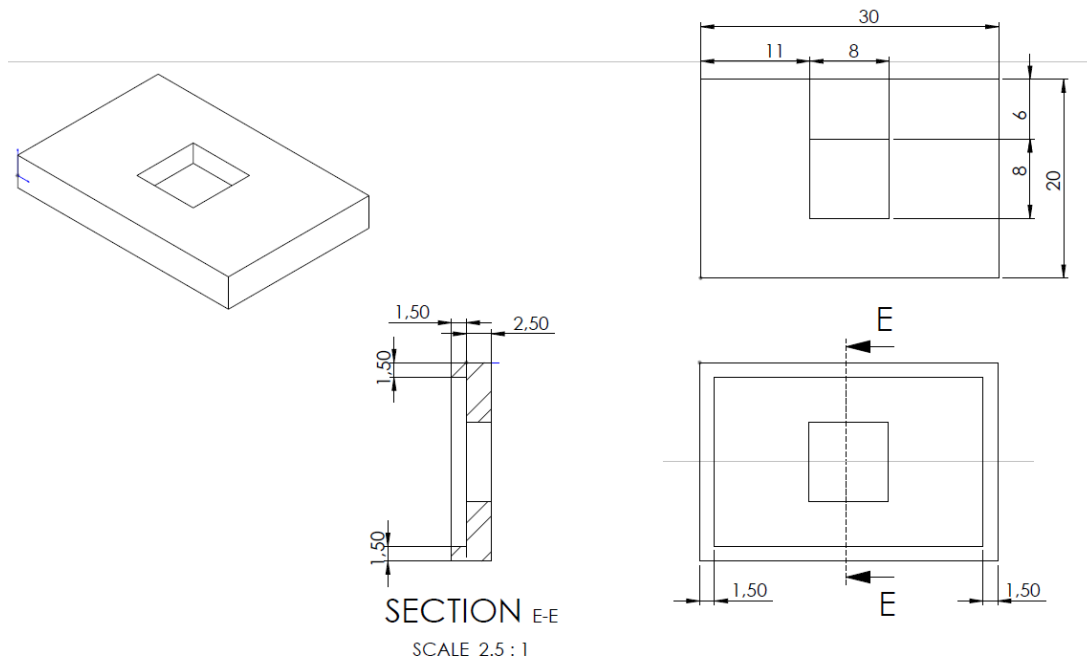
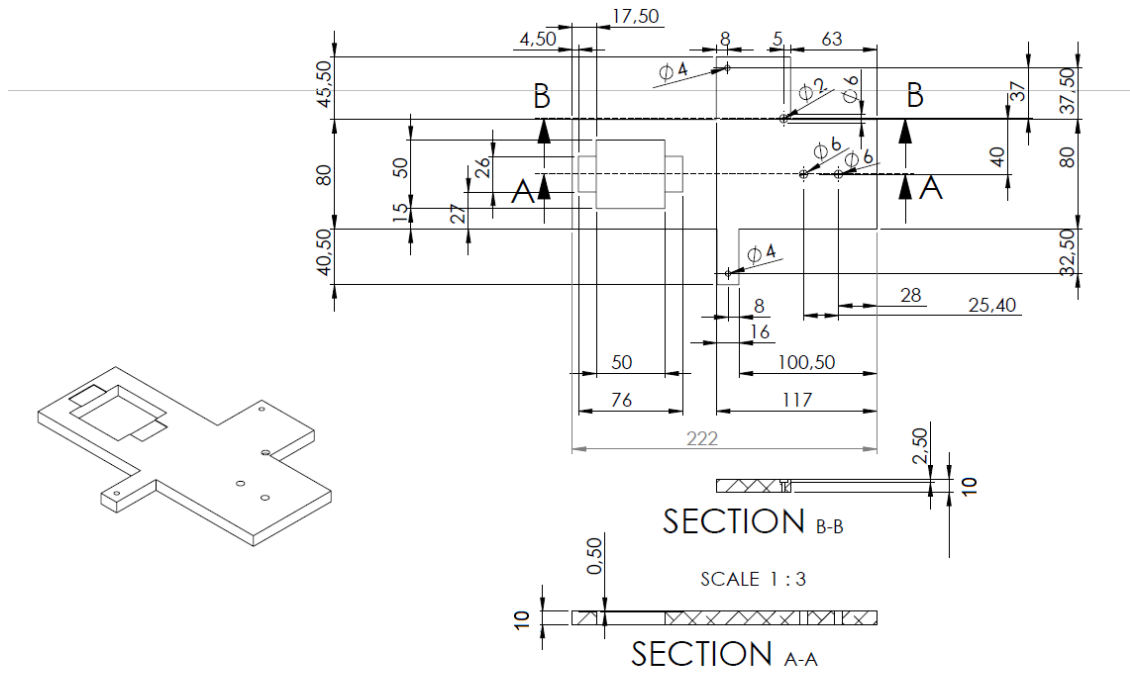
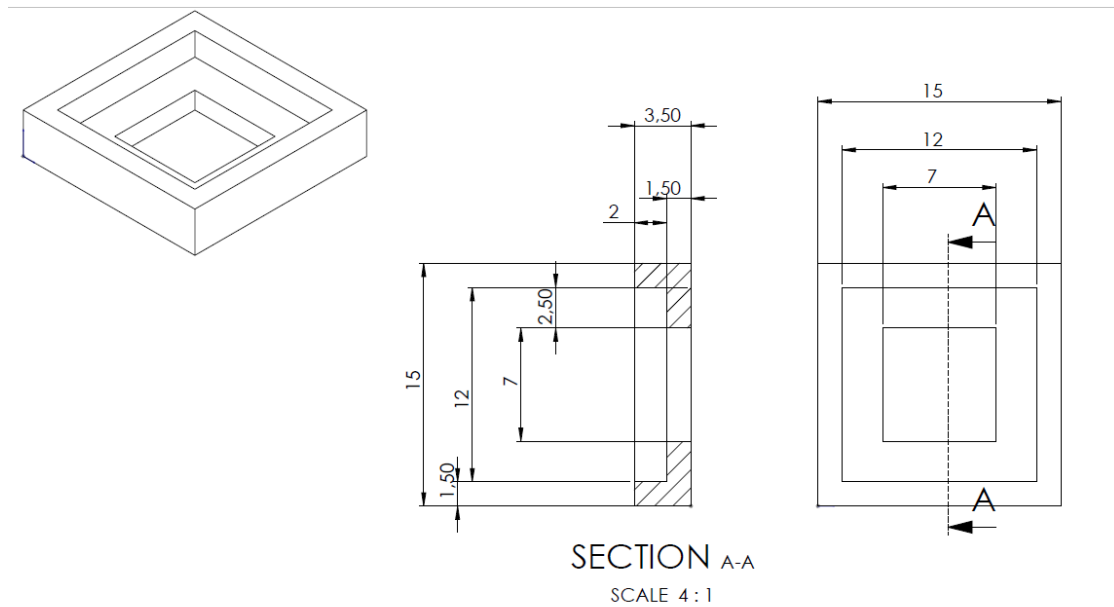


**Figure S3.** Drawing of the lid.



TU Delft Industrial Design Engineering	benaming	datum	groep	schaal	maateenheid
	Substraat houder_drawing	11-6-2019	Thesis ME- Babette Haitsma Muller (4404874)	1:1	mm
		getekend	groep	maat	gewicht
			Thesis ME- Babette Haitsma Muller (4404874)	A4	gram
					tekening nr. / opmerkingen b.a.haitsmamuller@student.tudelft.nl

Figure S4. Drawing of the substrate holder.



TU Delft Industrial Design Engineering	benaming	datum	groep	schaal	maateenheid
	Mal_drawing	26-6-2019	Thesis ME-BMD Babette Haitsma Muller (4404874)	1:1	mm
		getekend	groep	maat	gewicht
			Thesis ME-BMD Babette Haitsma Muller (4404874)	A4	gram
					tekening nr. / opmerkingen b.a.haitsmamuller@student.tudelft.nl

Figure S5. Drawing of the adhesive mold.

### S.1.3 Data analysis

#### *Time synchronization*

The MATLAB-script that is used to assign the right time values to the frames per experiment is inserted below.

```
1  % Graduation project: capturing fluid flow (drainage) on micropatterned samples
2  % Babette Haitzma Mulier (4404874)
3  % September/October 2019
4
5  % This script reads the time at which the screen recordings of the fluid flow
6  % are started from the videofiles, and the time at which the downward movement
7  % of the adhesive is started from the eventlogs, and corrects for this time difference.
8  % The videos are recorded with Bandicam-software on the computer that belonged
9  % to the Keyence microscope. The vertical stage is controlled by Thorlabs-software
10 % on a separate laptop. This script also corrects for the time difference
11 % between these two devices per day and during the day by linear interpolation.
12 % Ultimately, the frame nr. that corresponds to the point of contact can be
13 % matched among the tests.
14
15 - clear all
16 - close all
17 - clc
18
19
20 %% Save VideoInfo-file
21
22 - folder = 'G:/1. Video images';           % location of the main folder in which the video images of all experiments are stored in subfolders
23 - addpath(folder);                         % add folder to path
24 - S = dir(fullfile(folder, '*'));          % save the directory of the folder
25 - N = setdiff([S([S.isdir]).name], {'.', '..'}); % list of subfolders
26 - save('VideoInfo.mat', 'N');
27
28
29 %% Read date & time from the eventlogs and screen records
30
31 - folder = 'G:\Eventlogs\';                % location of the eventlogs
32 - addpath(folder);                         % add folder to path
33
34 % Store date and time of start sequence 3 from eventlogs
```

```

35 - S = dir(fullfile(folder, '**'));           % save the directory of the folder
36 - N = setdiff({S.name}, {'.', '..'});
37 - for kk = 1:numel(N)
38 -     FileDirectory = strcat(folder, N{kk});
39 -     T = importdata(FileDirectory);         %Load data from eventlog
40 -     Index = find(contains(T, 'PrepTest3 DOWN Sequence Started')); %Find index of string containing 'PrepTest3 DOWN Sequence Started'
41 -     Index = Index(length(Index), 1);      %Only store data of the last time sequence 3 started
42 -     InfoString = T(Index, 1);             %Store complete string
43 -     [EventDate(kk, 1), remain] = strtok(InfoString, ' '); %Filter date when the sequence started
44 -     EventTime(kk, 1) = strtok(remain, ' '); %Filter time when the sequence started
45 - end
46 - EventlogData = [N, EventDate, EventTime]; %Make matrix of the data
47
48
49 % Store date and time of start screen recording from movie-file
50 - folder = 'G:\';                          % location of the VideoInfo file
51 - addpath(folder);                          % add folder to path
52 - VideoInfo = load('VideoInfo');
53 - for ll = 1:length(VideoInfo.N)           % extract the test number and start date & time of the screen recording from the file name
54 -     InfoString = VideoInfo.N(1, ll);
55 -     [TestNumber(ll), remain] = strtok(InfoString, ' ');
56 -     [VideoDate(ll), remain] = strtok(remain, ' ');
57 -     [VideoTime(ll), remain] = strtok(remain, ' ');
58 - end
59 - TestNumber = TestNumber.';
60 - VideoDate = VideoDate.';
61 - VideoTime = VideoTime.';
62 - VideorecordingData = [TestNumber, VideoDate, VideoTime];
63
64
65 % Time conversion to ms
66
67 %EventTime
68 - for kk = 1:length(EventTime)

```



```

69 - [EventTime(kk,2),remain] = strtok(EventTime(kk,1),':');
70 - [DoubleDot,remain] = strtok(remain,'0123456789');
71 - [EventTime(kk,3),remain] = strtok(remain,':');
72 - [DoubleDot,remain] = strtok(remain,'0123456789');
73 - [EventTime(kk,4),remain] = strtok(remain,'.');
74 - [DoubleDot,remain] = strtok(remain,'0123456789');
75 - EventTime(kk,5) = remain;
76 - EventTime_ms(kk,1) = str2double(EventTime(kk,2))*60*60*1000 + str2double(EventTime(kk,3))*60*1000 ...
77 - + str2double(EventTime(kk,4))*1000 + str2double(EventTime(kk,5)); %Event time expressed in ms from midnight
78 - end
79 -
80 - %VideoTime
81 - for kk = 1:length(VideoTime)
82 - char -;
83 - [VideoTime(kk,2),remain] = strtok(VideoTime(kk,1),'-');
84 - [DoubleDot,remain] = strtok(remain,'0123456789');
85 - [VideoTime(kk,3),remain] = strtok(remain, '-');
86 - [DoubleDot,remain] = strtok(remain,'0123456789');
87 - [VideoTime(kk,4),remain] = strtok(remain, '-');
88 - [DoubleDot,remain] = strtok(remain,'0123456789');
89 - VideoTime(kk,5) = remain;
90 - VideoTime_ms(kk,1) = str2double(VideoTime(kk,2))*60*60*1000 + str2double(VideoTime(kk,3))*60*1000 ...
91 - + str2double(VideoTime(kk,4))*1000 + str2double(VideoTime(kk,5)); %Video time expressed in ms from midnight
92 - end
93 -
94 -
95 - %% Extract time difference between Keyence computer & laptop from excel-file
96 - % At the begin and end of each experiment day, the time on the Keyence computer and
97 - % laptop was registered 5x simultaneously and saved in the excel-file 'Experiment sequence'
98 -
99 - folder = 'G:\'; %Location of excel-file
100 - addpath(folder);
101 -
102 - [~,ExcelData] = xlsread('Experiment sequence.xlsx','Time Details'); %Load tab with time details from excel file

```

```

103 - ExcelData(1:127,:) = []; %Delete all rows corresponding to wrong tests and pilot tests
104 - ExcelDay(:,1) = ExcelData(:,1); %Extract day info
105 - ExcelDay = ExcelDay(~cellfun('isempty',ExcelDay)); %Delete all empty rows
106
107
108 % Separate begin & end time per day on laptop & Keyence from the excel-data
109 - [LaptopDay(:,1), LaptopTime(:,1)] = strtok(ExcelData(:,2), ' ');
110 - LaptopDay = LaptopDay(1:12:end);
111 - [Rest, LaptopTime(:,1)] = strtok(LaptopTime,'0123456789');
112 - KeyenceTime(:,1) = ExcelData(:,3);
113
114
115 % Time conversion to ms
116
117 % Laptop
118 - for kk = 1:length(LaptopTime)
119 -     [LaptopTime(kk,2),remain] = strtok(LaptopTime(kk,1), ':'); %extract hours
120 -     [DoubleDot,remain] = strtok(remain,'0123456789');
121 -     [LaptopTime(kk,3),remain] = strtok(remain, '.'); %extract minutes
122 -     [DoubleDot,remain] = strtok(remain,'0123456789');
123 -     [LaptopTime(kk,4),remain] = strtok(remain, '.'); %extract seconds
124 -     [DoubleDot,remain] = strtok(remain,'0123456789');
125 -     LaptopTime(kk,5) = remain; %extract milliseconds
126 -     LaptopTime_ms(kk,1) = str2double(LaptopTime(kk,2))*60*60*1000 + str2double(LaptopTime(kk,3))*60*1000 ...
127 -         + str2double(LaptopTime(kk,4))*1000 + str2double(LaptopTime(kk,5)); %Laptop time expressed in ms from midnight
128 - end
129
130 % Keyence
131 - for kk = 1:length(KeyenceTime)
132 -     [KeyenceTime(kk,2),remain] = strtok(KeyenceTime(kk,1), 'u'); %extract hours
133 -     [Rest,remain] = strtok(remain,'0123456789');
134 -     [KeyenceTime(kk,3),remain] = strtok(remain, 'm'); %extract minutes
135 -     [Rest,remain] = strtok(remain,'0123456789');
136 -     [KeyenceTime(kk,4),remain] = strtok(remain, 's'); %extract seconds

```

```

137 - [Rest,remain] = strtok(remain,'0123456789');
138 - KeyenceTime(kk,5) = strtok(remain,'m'); %extract milliseconds
139 - KeyenceTime_ms(kk,1) = str2double(KeyenceTime(kk,2))*60*60*1000 + str2double(KeyenceTime(kk,3))*60*1000 ...
140 - + str2double(KeyenceTime(kk,4))*1000 + str2double(KeyenceTime(kk,5)); %Keyence time expressed in ms from midnight
141 - end
142
143
144 % Store average time difference between Keyence & laptop of the begin and end time of a day
145 - Timediff = KeyenceTime_ms - LaptopTime_ms;
146 - Timediff(isnan(Timediff))=[]; %Delete the nan-values in the vector
147 - Timediff_avg = movmean(Timediff,[(5-1) 0]); %Take from every set of 5 rows the average
148 - Timediff_avg = Timediff_avg(5:5:end,:); %Store the average of rows 1-5, 6-10, etc. (so per begin/end of the day)
149 - Timediff_begin = Timediff_avg(1:2:end);
150
151 % Store coefficients for linear interpolation
152 - Timediff_day = diff(Timediff_avg); %Take time difference per set of two rows (= begin and end of a day)
153 - Timediff_day = Timediff_day(1:2:end); %Store the difference of rows 1-2, 3-4, etc. (time difference between begin and end of the day)
154
155 - KeyenceTime_ms(isnan(KeyenceTime_ms)) = []; %Delete the nan-values in the vector
156 - KeyenceTime_avg = movmean(KeyenceTime_ms,[(5-1) 0]); %Take from every set of 5 rows the average
157 - KeyenceTime_avg = KeyenceTime_avg(5:5:end,:); %Store the average of rows 1-5, 6-10, etc. (so per begin/end of the day)
158 - KeyenceTimediff_day = diff(KeyenceTime_avg); %Take time difference per set of two rows
159 - KeyenceTimediff_day = KeyenceTimediff_day(1:2:end); %Store the difference of rows 1-2, 3-4, etc. (time difference between begin and end of the day)
160 - Direction_coefficient = Timediff_day./KeyenceTimediff_day; %Relation between time difference on laptop and Keyence per day
161
162 - KeyenceTime_begin = KeyenceTime_avg(1:2:end); %Start of the day (time on laptop)
163
164 - Interpol_coeff = [KeyenceTime_begin, Direction_coefficient, Timediff_begin]; %Rows correspond to same rows as in variable LaptopDay
165
166
167 %% Store time difference between laptop and Keyence per test by linear interpolation during the day
168
169 - ii = 14; %adapt per day; ii corresponds to a specific day (same rows as in 'LaptopDay'-variable)
170 - jj = 100; %adapt per test; jj corresponds to the order of videos in folder '1. Video images'

```

171 -	kk = 141;      %%adapt per test; kk is the video number	
172 -	deltaT(jj) = VideoTime_ms(jj) - Interpol_coeff(ii,1);	%Time between begin of test day and begin of experiment
173 -	KeyLaptop_diff(jj) = Interpol_coeff(ii,2)*deltaT(jj) + Interpol_coeff(ii,3);	%Linear interpolation (y = ax+b) of time difference laptop-keyence
174		%between begin and end of the day
175 -	ReactionTime(jj,1) = KeyLaptop_diff(jj) - (VideoTime_ms(jj) - EventTime_ms(kk));	%Time [ms] between start screen record and movement of microstage per test;
176		%rows correspond to order of files in folder '1. Video images'
177		
178	%% Store #frames between start video & start movement microstage	
179		
180 -	framerate = 60;	%[fps]
181 -	ReactionTime(:,2) = floor(ReactionTime(:,1)*framerate/1000) + 1;	%Amount of frames that are recorded before the vertical microstage started moving;
182		%assumption: the video begins recording at time 0.00s.
183		
184	%% Save ReactionTime-variable	
185		
186 -	save('ReactionTime.mat','ReactionTime');	

## Pre-processing

The MATLAB-script that is used to pre-process the drainage data is inserted below.

```
1  % Graduation project: capturing fluid flow (drainage) on micropatterned samples
2  % Babette Haitsma Mulier (4404874)
3  % July 2019
4  |
5  % This scripts reads .jpeg-images of the fluid flow and pre-processes
6  % these before they can be processed with PIVlab-software. The fluid flow
7  % is measured with 3um particles and the Keyence VHX 6000 microscope.
8
9 - clear all
10 - close all
11 - clc
12
13
14 %% Enter geometrical properties per experiment
15
16 - d = 80; %diameter of pillars [um]
17 - s = 20; %spacing between pillars [um]
18 - x0 = 1319; %circle center x-coordinate of pillar bottom right [px]
19 - y0 = 878; %circle center y-coordinate of pillar bottom right [px]
20 - threshold = 0.585; %binarization threshold (manually determined)
21
22
23 %% Convert geometrical properties into amount of pixels per frame
24
25 - if d == 80 && s == 40 %um
26 -     diam = 168; spacing = 80; %pixels
27 - elseif d == 80 && s == 20
28 -     diam = 168; spacing = 42;
29 - elseif d == 40 && s == 20
30 -     diam = 82; spacing = 42;
31 - else diam = 0; spacing = 0;
32 - end
33
34 - radius = diam/2;
```

```

35
36
37 %% Define positions of pillars/masks
38
39 x0 = [x0:-2*radius-spacing:radius+1].'; % x-positions of the centre of all pillars
40 y0 = [y0:-2*radius-spacing:radius+1].'; % y-positions of the centre of all pillars
41
42 for i = 1:length(x0)
43     x(i,:) = (x0(i)-radius):(x0(i)+radius); % all x-positions of the perimeter of the pillars
44 end
45 y = sqrt(radius^2-(x(1,:)-x0(1)).^2); % defining the trend of the pillar/circle
46 for i = 1:length(y0)
47     y1(i,:) = round(y) + y0(i);
48     y2(i,:) = y0(i) - round(y);
49 end
50
51
52 %% Read .jpeg-files of all tests and binarize them.
53 % Files of one test are saved in one subfolder. All subfolders are saved in one main folder.
54
55 folder = 'G:/1. Video images'; % location of the main folder in which the video images of all experiments are stored in subfolders
56 addpath(folder); % add folder to path
57 S = dir(fullfile(folder,'*')); % save the directory of the folder
58 N = setdiff({S([S.isdir]).name},{'','..'}); % list of subfolders
59
60 % Definitions
61 Framerate = 60; % frames per second
62 folderBinarized = 'G:/2. Binarized images - unique frames incl. mask - 4s before till 3s after contact/';
63
64 % Loop through the subfolders
65 for ii = 82
66     T = dir(fullfile(folder, N{ii},'*')); % test nr. (corresponding with order in 'folder'-directory)
67     C = {T(~[T.isdir]).name}; % specify the file extension
68     NewFolderName{ii} = strtok(N{ii},' '); % amount of files (frames) in subfolder

```

```

69 - FileDirectory = strcat(folderBinarized,NewFolderName{ii});
70 - mkdir(sprintf(FileDirectory)); % Generate subfolder per experiment for binarized images
71 - p = zeros(1047,1440); % create an empty p-vector
72 - kk = 1;
73
74 % Save framenumbers, corresponding time points and separation distance, from the begin of the microstage movement
75 - load('ReactionTime.mat'); % Includes the nr. of frames between starting a video and starting the
76 % movement of the microstage (generated by script 'Time_trial')
77 - Frames_till_movement = ReactionTime(ii,2);
78 - Frames_from_start_movement = numel(C)-Frames_till_movement;
79 - Time = linspace(0,Frames_from_start_movement/Framerate, Frames_from_start_movement); % Time vector [s]
80 - Separation_dist = [linspace(1.5,0,1.5/0.05*60),zeros(1,Frames_from_start_movement-1800)]; % Separation distance [mm] in time
81 - Framenr_corr_time_sepdist{ii}(:, :) = [(Frames_till_movement+1):numel(C); Time; Separation_dist]; % Vector with the framenumbers and their corresponding points in time and
82 % separation distance
83
84 - Begin_frame = Framenr_corr_time_sepdist{ii}(1,1800) - 4*Framerate; % Corresponding with 4s before calibrated contact
85 - End_frame = Begin_frame + 7*Framerate; % Corresponding with 3s after calibrated contact
86
87 - load('Framenr_time_sepdist.mat');
88
89 % Loop through the files in a subfolder
90 - for jj = Begin_frame:End_frame % frames to be analysed
91 - F = fullfile(folder, N{ii}, C{jj}); % get the exact file location
92 - picture = imread(F); % read .jpeg-file
93 - I = rgb2gray(picture); % convert picture from colour to grey scale
94
95 % Extract pillars from analysis = apply 'masks' to cover the pillars
96 - for i = 1:length(x0)
97 - for j = 1:length(y0)
98 - for k = 1:length(x)
99 - I(y2(j,k):y1(j,k),x(i,k)) = 255;
100 - end
101 - end
102 - end

```

```

103
104 % Remove air bubble(s)/pillar cluster(s)
105 - I(705:795,1183:1273) = 255; % adapt location manually per test
106 - I(872:1080,1309:1440) = 255; % adapt location manually per test
107 % I(917:1016,1128:1203) = 255;
108 % I(769:870,431:473) = 255;
109
110 % Crop images % for same relative position of pillars in all videos: bottom right pillar exactly in bottom right corner
111 - I(1:33,:) = []; % crop image: delete watermark Bandicam
112 - I(:,1441:1920) = []; % crop image: delete side bar
113 - Ix = size(I,1); % Original #rows
114 - Iy = size(I,2); % Original #columns
115 - Ix_new = Ix - 250; % Allowed #rows (250 = max. # of pixels that are removed in next step = diam + spacing d80s40)
116 - Iy_new = Iy - 250; % Allowed #columns
117 - I((y0(1) + radius - 33):end,:) = []; % Delete rows beneath bottom pillars (-33 because of previous cropping)
118 - I(:,(x0(1) + radius):end) = []; % Delete columns right to most right pillars
119 - I(1:(size(I,1) - Ix_new),:) = []; % Crop such that every experiment has same image size
120 - I(:,1:(size(I,2) - Iy_new)) = []; % " "
121
122 % Binarize images (filter particles in depth-of-field region (in focus) based on grey value)
123 - bw = imbinarize(I,threshold);
124
125 % Save the binarized images of a test in the previously created subfolder if they are not completely white (test not yet begun)
126 - if mean(bw(:)) < 1 && isequal(bw,p) == 0 % if at least one pixel is black (not white) and if the current picture is not identical to the previous
127 % picture(s), save the picture
128 - folderFile = FileDirectory; % folder-directory in which the binarized images of a test should be saved
129 - baseFileName = sprintf('00%02d.jpg',jj); % get the base file name
130 - fullFileName = fullfile(folderFile, baseFileName); % combine it with the folder to get the full filename.
131 - imwrite(bw, fullFileName); % write bw-values to a black-and-white image for further analysis
132 - p = bw;
133 - Framenr_time_sepdist{ii}(:,kk) = Framenr_corr_time_sepdist{ii}(:,jj-Frames_till_movement); % Only includes framenumbers of unigie frames and their corresponding
134 % time and separation distance vectors
135 - kk = kk+1;
136 - end
137 - end
138 - end
139
140 - save('Framenr_time_sepdist.mat','Framenr_time_sepdist');

```



## Post-processing

The MATLAB-script that is used to extract the velocity data of the particle flow from the output of the PIV-analysis, filter the noise, and plot the results is inserted below.

```
1  % Graduation project: capturing fluid flow (drainage) on micropatterned samples
2  % Babette Haitzma Mulier (4404874)
3  % July 2019 - February 2020
4
5  % This scripts extracts the velocity data of the particle flow from the
6  % output of the PIV-analysis (.txt-files), filters the noise and plots
7  % the results (absolute average velocity & standard deviation).
8
9  clear all
10 close all
11 clc
12
13
14 Testnr = 74;                %%Adapt {nr.} in accordance with test (numbers correspond to order of folders in folder '1. Video images')
15
16
17 %% DEFINITIONS
18 %% Load data and generate vectors
19
20 load('Framenr_time_sepdist.mat');    % File containing the framenumbers of the non-identical frames and their corresponding points in time and the separation distance
21
22 Framenr_time_sepdist(Testnr)(:,6:7) = [];    %%Remove frames that are excluded from PIV-analysis manually
23
24 % Time-vector
25 t = Framenr_time_sepdist(Testnr)(2,:);    % Extract time info from file
26 t = t - t(1) - 4;    % Adapt the timescale (first frame is 4s before calibrated contact). The point of calibrated contact is always at 0s.
27 t = movmean(t,[0 (2-1)]);    % Take from every set of 2 time points the average (the flow velocity in PIVlab is also calculated by comparison of two frames)
28 t(end) = [];    % Remove last value (cannot be averaged)
29
30 % Separation distance-vector
31 delta = Framenr_time_sepdist(Testnr)(3,:);    % Extract separation distance info from file
32 delta = movmean(delta,[0 (2-1)]);    % Take from every set of 2 data points the average (the flow velocity in PIVlab is also calculated by comparison of two frames)
33 delta(end) = [];    % Remove last value (cannot be averaged)
34
```

```

35 % Conversion factor pix/frame to m/s
36 mppixel = 100.00e-6/219; % Calibration: meter per pixel (scale bar is 100.00um and corresponds to 219 pixels in horizontal direction)
37 spframe{Testnr} = Framenr_time_sepdist{Testnr}(2,2:end) - Framenr_time_sepdist{Testnr}(2,1:end-1); % Time [s] between two non-identical frames
38
39
40 %% EXTRACT DATA
41 %% Read .txt-files
42
43 folder = 'G:\3. Txt-files'; % Location of the .txt-files
44 addpath(folder); % add folder to path
45 S = dir(fullfile(folder,'*')); % save the directory of the folder
46 N = setdiff({S([S.isdir]).name},{'.','..'},'sorted'); % list of subfolders (tests)
47
48 for ii = 9 % loop through the subfolders (one by one)
49     T = dir(fullfile(folder, N{ii},'*')); % specify the file extension
50     C = {T(~[T.isdir]).name}; % .txt-files per test (in subfolder)
51     for jj = 1:numel(C) % loop through the files in a subfolder
52         F = fullfile(folder, N{ii}, C{jj}); % get the exact file location
53         file_info(:, :) = csvread(F,3,0); % Collect data
54
55         % Store the data in tables. Rows: amount of pixels, Columns: amount of frames per movie, 3D: amount of movies.
56         u_vel(:,jj,ii) = file_info(:,3)*mppixel*1/spframe{Testnr}(jj); % Convert velocity in x-direction [pix/frame] to [m/s]; definition: positive x-velocity is to the right
57         v_vel(:,jj,ii) = -file_info(:,4)*mppixel*1/spframe{Testnr}(jj); % Convert velocity in y-direction [pix/frame] to [m/s]; definition: positive y-velocity is upwards
58         abs_vel(:,jj,ii) = sqrt(u_vel(:,jj,ii).^2 + v_vel(:,jj,ii).^2); % Absolute velocity of the particles
59     end
60 end
61
62
63 %% Store the average of the absolute particle velocity per frame/time unit
64
65 abs_vel_average = nanmean(abs_vel); % Absolute average velocity of the particles in a frame, after removing the NaN-values
66
67 %% Suppress 1 of the 2 following options
68 %% 1. Data in the first folder of folder '3. Txt-files'

```

```

69 - abs_vel_average = [squeeze(abs_vel_average); t]; % Data in the first folder is organized in rows
70
71 %%2. Data from the second folder onwards of folder '3. Txt-files'
72 - abs_vel_average = squeeze(abs_vel_average); % Data from the second folder onwards is organized in columns
73 - abs_vel_average(:,1:ii-1) = []; % Remove ... columns (when analysing one folder per time)
74 - abs_vel_average = [abs_vel_average.'; t]; % Convert columns to rows
75
76 - save('G:/4. Velocity data/Test114_absvelavg_vs_time_uniqueframes.mat','abs_vel_average'); %%Adapt per test; save the abs. avg. velocity and corresponding time as row vectors
77
78
79 %% Remove noise - low-pass filter
80
81 - abs_vel_avg_lowpass(1,:) = lowpass(abs_vel_average(1,:),5,60); % Low-pass filter that samples 'abs_vel_average' at a rate of 60Hz, with a passband frequency of 5Hz
82 - abs_vel_avg_lowpass(2,:) = t;
83 - save('G:/4. Velocity data/Test114_absvelavg_vs_time_uniqueframes_lowpass.mat','abs_vel_avg_lowpass'); %%Adapt per test; save the abs. avg. velocity and corresp. time as
84 %row vectors
85
86 %% PLOTS
87 %% Single plots
88
89 - figure; % Plot with data of one test
90 - plot(abs_vel_avg_lowpass(2,:),abs_vel_avg_lowpass(1,:)); % Velocity vs. time
91 - title('Absolute average velocity in time','fontsize',22);
92 - xlabel('Time [s]','fontsize',18);
93 - ylabel('Absolute average velocity [m/s]','fontsize',18);
94 - set(gca,'FontSize',18)
95
96
97 %% Combined plots
98 % Compare the absolute average velocities in time among the test conditions
99
100 %%D00s20 glass medium height (all frames)
101 - Test039 = load('Test039_absvelavg_vs_time_uniqueframes_lowpass.mat');
102 - Test039 = Test039.abs_vel_avg_lowpass;

```

```

103 - Test062 = load('Test062_absvelavg_vs_time_uniqueframes_lowpass.mat');
104 - Test062 = Test062.abs_vel_avg_lowpass;
105 - Test091 = load('Test091_absvelavg_vs_time_uniqueframes_lowpass.mat');
106 - Test091 = Test091.abs_vel_avg_lowpass;
107 - Test107 = load('Test107_absvelavg_vs_time_uniqueframes_lowpass.mat');
108 - Test107 = Test107.abs_vel_avg_lowpass;
109 - Test123 = load('Test123_absvelavg_vs_time_uniqueframes_lowpass.mat');
110 - Test123 = Test123.abs_vel_avg_lowpass;
111
112 %%D80s20 PDMS medium height (skipped every 2nd frame)
113 - Test038 = load('Test038_absvelavg_vs_time_uniqueframes_lowpass.mat');
114 - Test038 = Test038.abs_vel_avg_lowpass;
115 - Test071 = load('Test071_absvelavg_vs_time_uniqueframes_lowpass.mat');
116 - Test071 = Test071.abs_vel_avg_lowpass;
117 - Test073 = load('Test073_absvelavg_vs_time_uniqueframes_lowpass.mat');
118 - Test073 = Test073.abs_vel_avg_lowpass;
119 - Test105 = load('Test105_absvelavg_vs_time_uniqueframes_lowpass.mat');
120 - Test105 = Test105.abs_vel_avg_lowpass;
121 - Test114 = load('Test114_absvelavg_vs_time_uniqueframes_lowpass.mat');
122 - Test114 = Test114.abs_vel_avg_lowpass;
123
124
125 - figure;
126 - plot(Test039(2,:),Test039(1,:), '--',Test062(2,:),Test062(1,:), '--',Test091(2,:),Test091(1,:), '--',Test107(2,:),Test107(1,:), '--',Test123(2,:),Test123(1,:), '--','LineWidth',2);
127 - hold on
128 - plot(Test038(2,:),Test038(1,:),Test071(2,:),Test071(1,:),Test073(2,:),Test073(1,:),Test105(2,:),Test105(1,:),Test114(2,:),Test114(1,:), 'LineWidth',2);
129 - title('Absolute average velocity in time','fontsize',20);
130 - xlabel('Time [s]','fontsize',16);
131 - ylabel('Absolute average velocity [m/s]','fontsize',16);
132 - %legend('Test039','Test062','Test091','Test107','Test123','Test038','Test071','Test073','Test105','Test114','fontsize',16); %%Adapt per plot
133 - legend('Glass\1','Glass\2','Glass\3','Glass\4','Glass\5','PDMS\1','PDMS\2','PDMS\3','PDMS\4','PDMS\5','fontsize',16);
134 - set(gca,'FontSize',16)
135
136
137 %% STANDARD DEVIATION
138 %% Compare the results in time among the test conditions
139
140 - std_vel = std(abs_vel_avg_lowpass(1:),'omitnan'); % Standard deviation of the filtered absolute average velocity, while omitting NaN-values
141 - std_vel = squeeze(std_vel);
142
143 - figure;
144 - plot(t,std_vel(1,:));
145 - title('Standard deviation of the absolute average velocity in time','fontsize',20);
146 - xlabel('Time [s]','fontsize',16);
147 - ylabel('Standard deviation [m/s]','fontsize',16);
148 - %legend(' ','fontsize',16);
149 - set(gca,'FontSize',16);

```

### S.1.4 Results

**Table S1.** A categorization of the main flow direction per experiment. The experiment conditions are expressed in the format *adhesive\_substrate\_focal plane*. The abbreviations for the focal planes correspond with the tip (X), half-way (M) and the onset (BL) of the adhesive's micropillars (p.o.c. = point of contact).

Flow direction (towards...)	Experiment condition (experiment nr.)
North	<p>D80s20_pdms_X (044; left side deflects north-west; right side deflects north-east)</p> <p>D80s20_pdms_BL (046; flows around the air bubble)</p> <p>D40s20_pdms_M (089; just before contact the flow bounces shortly to the west, and then again shortly to north; flow stops abruptly after p.o.c.)</p> <p>D40s20_gls_BL (106; before focus flow to south-east, then zigzag to north, and after p.o.c. to east)</p> <p>D80s40_pdms_BL (111; flow deflects to west at the left side of the field of view; flow stops abruptly after p.o.c.)</p> <p>D40s20_pdms_M (113; flow stops abruptly after p.o.c.)</p> <p>D80s20_pdms_BL (115; flow zigzags before focus; fluid flows around air bubble; flow bounces to south after p.o.c.)</p> <p>D40s20_gls_X (116; flow stops abruptly after p.o.c.)</p> <p>D80s40_pdms_BL (120; fluid flows around air bubble; flow bounces southwards after p.o.c.)</p> <p>D80s40_gls_X (121; just before p.o.c. the fluid abruptly deflects fast to the west; flow stops abruptly after p.o.c.)</p> <p>D80s20_gls_M (123; just before p.o.c. flow zigzags in multiple directions; after p.o.c. slow flow to north-west)</p> <p>D80s20_gls_X (138; it seems that the fluid flows in another direction before focus = p.o.c.; flow stops abruptly after p.o.c.)</p>
North-east	<p>D80s20_pdms_M (038; abruptly deflects southwards after p.o.c.)</p> <p>D40s20_pdms_M (043)</p> <p>D80s20_gls_BL (047; first fluid moves like it doesn't know where to go (zigzag))</p> <p>D80s20_pdms_M (071; just before p.o.c. short bounce in west direction followed by no flow)</p> <p>D80s20_pdms_M (073; fast flow in straight path to east + slow flow in semi-wave pattern to north-east)</p> <p>D40s20_pdms_BL (077)</p> <p>D80s40_pdms_M (087)</p> <p>D80s20_pdms_BL (101; mixed with flow to the east)</p> <p>D40s20_pdms_BL (102; flow stops abruptly after p.o.c.)</p> <p>D80s20_pdms_M (105; fluid flows around air bubble; flow stops abruptly after p.o.c.)</p> <p>D80s40_gls_BL (112; zigzag path to north-east, then abruptly moves to west)</p> <p>D80s40_pdms_X (136; the flow direction was south-west just before focus = p.o.c., and shortly bounces to north-east just after p.o.c.; flow quickly slows down after p.o.c.)</p> <p>* Many conditions with PDMS as substrate, including 4 out of 5 d80s20_pdms_M-measurements</p>
East	<p>D80s40_pdms_BL (057; flow alters between south and east like a zigzag; flows around air bubble; flow stops abruptly after p.o.c.)</p>

	<p>D80s20_pdms_BL (065)  D40s20_pdms_X (067)  D80s40_pdms_M (068; some fluid slowly flows one pillar downwards whereafter it is absorbed by the fast eastward flow; only flow after p.o.c.)  D80s20_gls_X (078; flow stops after p.o.c.)  D40s20_gls_X (108; flow seems to start after p.o.c.)  D40s20_gls_M (109; flow seems to start after p.o.c.)  D80s20_pdms_M (114)  D80s20_gls_BL (118; fluid flows around air bubbles)  D80s20_gls_X (125; flow seems to flow north before focus, and the abruptly changes direction when in focus)</p>
South-east	<p>D40s20_gls_BL (034; abruptly deflects to north after p.o.c.)  D80s40_gls_M (042; flow stops abruptly after p.o.c.)  D40s20_gls_BL (051; after p.o.c. short bounce in the opposite direction followed by no flow)  D80s40_pdms_BL (090; it seems that the flow direction was north-east before the flow was in focus; flow stops abruptly after p.o.c.; flow through air bubble)  D80s40_gls_BL (130; flow suddenly changes to north-west just before contact and then slows down)</p> <p>* Many conditions are on glass and focus on the backing layer.</p>
South	<p>D40s20_gls_X (045; flow stops abruptly after p.o.c.)  D80s20_gls_M (091; fluid flows around air bubble; just before contact zigzag path and a short fast bounce to the west; flow stops abruptly after p.o.c.)</p>
South-west	<p>D40s20_pdms_X (036; flow stops abruptly after p.o.c.)  D80s40_pdms_M (037; deflects southwards after p.o.c.)  D80s20_gls_X (041; flow stops abruptly after p.o.c.)  D80s40_pdms_BL (049; flow stops abruptly after p.o.c.)  D40s20_pdms_M (052; after p.o.c. slow flow to south-east)  D80s40_pdms_X (055; flow stops abruptly after p.o.c.)  D80s40_gls_X (069; flow quickly slows down at p.o.c.)  D40s20_gls_BL (075; zigzag path; flow stops abruptly after p.o.c.)  D80s40_pdms_X (082; flow stops abruptly after p.o.c.)  D80s20_gls_BL (093; fluid flows to north-east when still out of focus before contact; flow slows down at p.o.c., after that shortly accelerates to south-west)  D80s40_pdms_X (094; flow stops abruptly after p.o.c.)  D80s40_gls_X (098; flow quickly slows down after p.o.c.)  D80s40_pdms_M (126; fluid flows through/around air bubbles; flow stops abruptly after p.o.c.)  D80s40_pdms_X (127; flow stops abruptly after p.o.c.)  D40s20_pdms_BL (128; flow abruptly changes to south-east after p.o.c.)  D40s20_pdms_X (129; flow stops abruptly after p.o.c.)  D40s20_pdms_BL (137; flow stops abruptly after p.o.c.)  D40s20_pdms_BL (139; flow stops abruptly after p.o.c.)  D80s20_pdms_X (141; flow stops abruptly after p.o.c.)</p>
West	<p>D80s40_gls_BL (033; abruptly deflects southwards after p.o.c.)  D80s40_gls_BL (059; flow stops abruptly after p.o.c.)  D80s20_gls_M (062; flow stops abruptly after p.o.c.)  D40s20_gls_M (070; flow stops abruptly after p.o.c.)  D80s40_gls_BL (083; it seems that the flow first flowed eastwards)  D40s20_gls_X (084; flow stops abruptly after p.o.c.)</p>

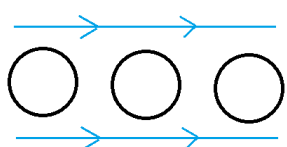
	<p>D80s40_gls_X (086; flow quickly slows down after p.o.c.)  D40s20_gls_M (088; only flow at p.o.c.)  D80s40_gls_M (095; flow quickly slows down after p.o.c.)  D80s20_gls_X (104; it seems that the flow direction was east just before focus, and shortly bounces to west just before p.o.c.; flow through air bubble; flow stops abruptly after p.o.c.)  D8040_gls_M (119; before focus the flow seems to flow eastwards and abruptly changes direction when in focus; flow quickly slows down after p.o.c.)  D40s20_gls_M (124; flow quickly slows down/stops after p.o.c.)  D40s20_gls_M (134; flow stops abruptly after p.o.c.)  D80s40_gls_M (140; fluid flows around air bubble; slightly mixed with flow to north; flow quickly slows down after p.o.c.)</p> <p>* All experiments are on glass. All planes with focus on backing layer are combined with a d80s40-adhesive. 4 out of 5 d40s20_gls_M-measurements have flow in this direction.</p>
North-west	<p>D80s40_gls_M (058; mixed with flow to the west; flow stops abruptly after p.o.c.)  D80s20_pdms_X (063; fluid abruptly flows to north-east just before contact for a short time; flow stops abruptly after p.o.c.)  D80s40_pdms_M (097; bounces south-west just before contact; flow quickly slows down after p.o.c.)  D40s20_pdms_X (100; to the right side of the field of view the flow is mostly to the north; flow stops abruptly after p.o.c.)  D80s20_pdms_X (103; flow stops abruptly after p.o.c.)  D40s20_pdms_M (122; flow stops abruptly after p.o.c. and slowly bounces back south-east)  D40s20_gls_BL (131; it seems that the flow direction was east just before focus, and shortly bounces to north-west just before p.o.c.; flow stops abruptly after p.o.c.)  D80s40_gls_X (135; flow stops abruptly after p.o.c.)</p>
Radially outward	<p>D80s20_gls_M (039; from 1.5s before contact flow around the air bubble to the east; flow stops abruptly after p.o.c.)  D8020_pdms_BL (072; just before contact most of the fluid flows to north-east around air bubbles; flow stops abruptly after p.o.c.)</p>
Radially inwards	
Random	<p>D80s20_gls_BL (064; flow stops abruptly after p.o.c.)  D80s20_gls_BL (079; random movement, then flow bended to north and then west; flow stops after p.o.c.)  D80s20_gls_M (107; zigzag to west and east; zigzag stops after p.o.c.)</p> <p>* All d80s20 on glass</p>
No flow	<p>Unpatt_pdms_BL (035)  Unpatt_gls_BL (050)  D40s20_gls_X (053)  Unpatt_pdms_BL (054)  Unpatt_gls_BL (056)  Unpatt_pdms_BL (074)  D80s20_pdms_X (080)  D40s20_pdms_X (081)  Unpatt_gls_BL (092)</p>

Unpatt_pdms_BL (096) Unpatt_gls_BL (110) Unpatt_gls_BL (132) Unpatt_pdms_BL (133)
--




**Table S2.** A selection of experiments in which an abrupt change in flow direction took place, including the frame number and separation distance between adhesive and substrate at which this happened. The critical heights as defined by Gupta & Fréchet per adhesive pattern are also inserted.<sup>45</sup>

Experiment nr. (adhesive pattern)	Frame nr.	Separation distance ( $\mu\text{m}$ )	Critical height as reported by Gupta & Fréchet ( $\mu\text{m}$ )
104 (d80s20)	1840	12.5	32.16
106 (d40s20)	1748	85.0	38.13
119 (d80s40)	1830	23.3	38.13
125 (d80s20)	1837	15.0	32.16
131 (d40s20)	1760	54.2	38.13
136 (d80s40)	1837	5.8	38.13

**Table S3.** A categorization of the main flow trajectory per experiment. The experiment conditions are expressed in the format adhesive\_substrate\_focal plane. The abbreviations for the focal planes correspond with the tip (X), half-way (M) and the onset (BL) of the adhesive's micropillars (p.o.c. = point of contact).

Flow trajectory	Experiment condition (experiment nr.)
Straight path 	D80s40_gls_BL (033) D80s20_gls_M (039) D40s20_gls_X (045) D80s20_pdms_BL (046) D80s40_pdms_BL (057) D80s40_gls_BL (059) D80s20_gls_M (062) D80s20_pdms_BL (065; combination with semi-wave path) D40s20_pdms_X (067; particles near pillars follow semi-wave path) D80s40_pdms_M (068) D80s20_pdms_M (073; fast flow in straight path to east + slow flow in semi-wave path to north-east) D80s40_gls_BL (083) D80s40_gls_M (095) D40s20_gls_BL (106) D40s20_gls_X (108; fast flow in straight path to east + slow flow in semi-wave pattern to north-east) D40s20_gls_M (109) D80s40_pdms_BL (111; slightly mixed with (semi-)wave pattern) D40s20_pdms_M (113; slightly mixed with (semi-)wave pattern) D80s20_pdms_M (114; particles near pillars follow semi-wave path) D80s20_pdms_BL (115; particles near pillars follow semi-wave path; slightly mixed with wave path) D80s20_gls_BL (118; particles near pillars follow semi-wave path) D8040_gls_M (119; mixed with semi-wave path near pillars and with wave path)



	<p>D80s40_pdms_BL (120; particles near pillars follow semi-wave path)  D80s20_gls_X (125; particles near pillars follow semi-wave path)  D80s20_gls_X (138; tends to a combination with (semi-)wave path)  D80s40_gls_M (140; slightly mixed with wave path)</p> <p>* The fluid flows in one of the orthogonal directions (north, east, south, west) in all experiments</p>
<p>Semi-wave path</p> 	<p>D40s20_gls_BL (034; after contact straight path)  D80s40_gls_M (042)  D40s20_pdms_M (043)  D80s20_gls_BL (047)  D80s40_pdms_BL (049)  D40s20_gls_BL (051)  D40s20_pdms_M (052)  D80s40_pdms_X (055)  D80s40_gls_M (058; mixed with straight path to the west)  D80s20_pdms_M (071; followed by straight path to the west)  D8020_pdms_BL (072)  D40s20_gls_BL (075)  D40s20_pdms_BL (077)  D80s40_pdms_X (082)  D80s40_pdms_M (087)  D80s40_pdms_BL (090)  D80s20_gls_BL (093)  D80s40_pdms_M (097)  D40s20_pdms_X (100)  D80s20_pdms_BL (101; mixed with straight path to the east)  D80s20_pdms_M (105)  D80s40_gls_BL (112; followed by straight path to the west)  D40s20_pdms_M (122)  D80s40_pdms_X (127)  D80s40_gls_BL (130)  D80s40_gls_X (135)  D40s20_pdms_BL (137)  D40s20_pdms_BL (139; evt. combination with wave path)  D80s20_pdms_X (141)</p> <p>* The particles flow in non-orthogonal directions in all experiments (north-east, south-east, south-west, north-west)</p>
<p>Wave path</p> 	
<p>No flow</p> 	<p>Unpatt_pdms_BL (035)  Unpatt_gls_BL (050)  D40s20_gls_X (053)  Unpatt_pdms_BL (054)  Unpatt_gls_BL (056)  Unpatt_pdms_BL (074)  D80s20_pdms_X (080)</p>

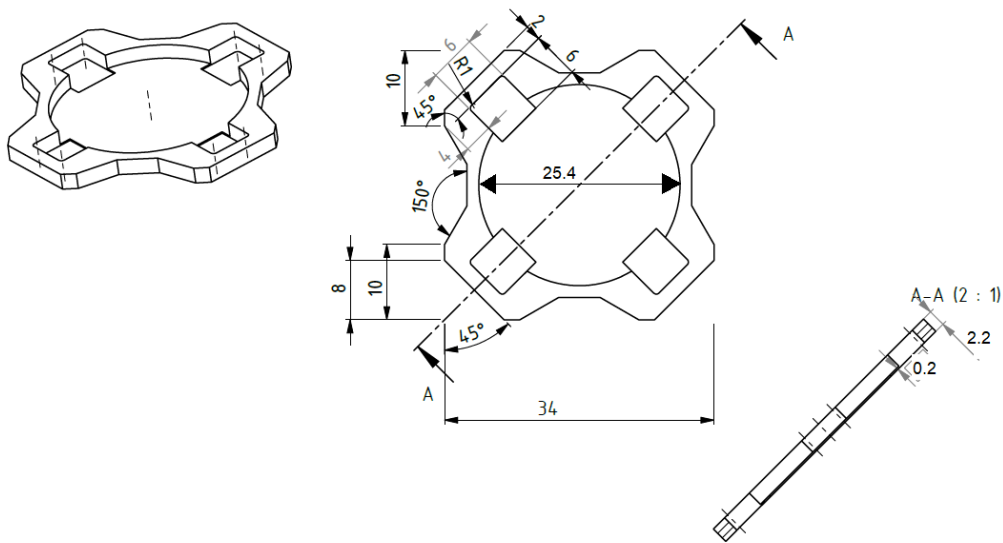
	D40s20_pdms_X (081) Unpatt_gls_BL (092) Unpatt_pdms_BL (096) Unpatt_gls_BL (110) Unpatt_gls_BL (132) Unpatt_pdms_BL (133)
Indistinguishable (too short flow path)	D40s20_pdms_X (036) D80s40_pdms_M (037; tends to flow around the pillars) D80s20_pdms_M (038; after p.o.c. straight) D80s20_glss_X (041) D80s20_pdms_X (044) D80s20_pdms_X (063) D80s40_gls_X (069) D40s20_gls_M (070) D80s20_gls_X (078) D40s20_gls_X (084) D80s40_gls_X (086) D40s20_gls_M (088) D40s20_pdms_M (089) D80s20_gls_M (091) D80s40_pdms_X (094) D80s40_gls_X (098; tends to semi-wave) D40s20_pdms_BL (102) D80s20_pdms_X (103) D80s20_gls_X (104) D40s20_gls_X (116) D80s40_gls_X (121) D80s20_gls_M (123; too fast flow) D40s20_gls_M (124) D80s40_pdms_M (126) D40s20_pdms_BL (128; tends to combination of straight and semi-wave paths) D40s20_pdms_X (129; tends to semi-wave) D40s20_gls_BL (131; tends to semi-wave) D40s20_gls_M (134; tends to be a combination of straight paths in the middle of the channels, and semi-wave paths near pillars) D80s40_pdms_X (136)
Random	D80s20_gls_BL (064) D80s20_gls_BL (079) D80s20_gls_M (107)

## S.2 PULL-OFF AND FRICTION

### S.2.1 Details of the setup

The substrate was attached to a holder that has a compartment of the same size as the diameter of the substrate. The holder on its turn was connected to a platform by magnets. The platform had the same size as the outer dimensions of the holder, such that the substrate was horizontally and vertically locked. The adhesive in the cantilever was locked in z-direction with a load of 1.96 N on top of the magnetic lid for practical reasons.

### S.2.2 Drawing



 Delft University of Technology	name	Sample cover adhesion				remark	b.a.haitsmamulier@stud
		H:\Desktop\				material	Staal
		units	mm	scale	1:1	quantity	2
		date	16-10-2019		mass	6.307 gr	
	author	Babette Haitsma Mulier (4404874)		group	Thesis	format	A4
							drawing no. <<drawing no.>>

Figure S6. Drawing of the substrate holder.

### S.2.3 Data analysis – pull-off

The MATLAB-script that is used to process the pull-off data is inserted below.

```
1 % Processing adhesion data of adhesives with 4 pattern geometries against
2 % substrates with 2 stiffnesses
3 % Babette Haitzma Mulier, Peter van Assenbergh
4 % February 2020
5
6 % This scripts reads data-files that include friction and adhesion forces
7 % of micropatterned samples against hemispherical substrates. This data is
8 % obtained on a customized setup.
9
10 clear all
11 close all
12 clc
13
14
15 %% Load files
16
17 load('datalist.mat') % the general properties of the friction and adhesion data (names, etc.)
18 load('data.mat') % the friction and adhesion data; columns correspond with the names in 'datalist.mat'
19 load('k_char_ad.mat') % characterization matrix for adhesion: converts displacement into forces
20
21 t=(1:20000)/1000; % Time [s]
22
23
24 %% Filter/smoothen and level the data & store the info in variables
25
26 e= 10; % filter at this frequency (1/e = 0.1 sec)
27 o= 2000; % sampling frequency
28 [B,A] = butter(2,e/(o/2),'low'); % /2 nyquist correction; high/low: remove data above/below 'e' Hz
29
30 for i = 1:length(files)
31 N = strsplit(files(i).name, '_'); % split name in parts;
32 UsedData(i).displacement = data.raw(:,i); % get corresponding displacement data
33 UsedData(i).leveled = data.raw(:,i)-mean(data.raw(1:300,i)); % subtract the initial displacement-value, for comparison among all experiments
34 UsedData(i).filtered = filtfilt(B,A,UsedData(:,i).leveled);
```

```

35 -     UsedData(i).names = files(i).name;           % removes auto generated time stamp from the name of the data
36 -     UsedData(i).pattern = N{1};
37 -     UsedData(i).substrate = N{2};
38 -     UsedData(i).test = N{3};
39 -     UsedData(i).repetition= N{4};
40 -     UsedData(i).signal = N{5};
41 - end
42
43
44 %% Extracting adhesion displacement data
45
46 % Data in x-direction
47 j=1;
48 for i = 1:length(UsedData)
49     if contains(UsedData(i).names, 'ad')*contains(UsedData(i).names, '_x') == 1
50         Adh(j).name = UsedData(i).names;
51         Adh(j).filt_x = UsedData(i).filtered;
52         j=j+1;
53     end
54 end
55
56 % Data in z-direction
57 j=1;
58 for i = 1:length(UsedData)
59     if contains(UsedData(i).names, 'ad')*contains(UsedData(i).names, '_z') == 1
60         Adh(j).filt_z=UsedData(i).filtered;
61         j=j+1;
62     end
63 end
64
65
66 %% Convert displacement data to force data & extract peak forces adhesion
67
68 for i = 1:length(Adh)

```

```

69 -     Adh(i).force_x = Adh(i).filt_z * k_char_ad(1,2) + Adh(i).filt_x * k_char_ad(2,2); % x-direction
70 -     Adh(i).force_z = Adh(i).filt_z * k_char_ad(1,1) + Adh(i).filt_x * k_char_ad(2,1); % z-direction
71 -     Adh(i).max = (max(-Adh(i).force_z)); % Peak force adhesion
72 - end
73
74
75 %% Representative adhesion force curves in time
76
77 % On glass
78 - figure(1);
79 - subplot(1,2,1)
80 - m=41; % test nr.
81 - plot(t,Adh(m).force_z)
82 - title('Pull-off on glass','fontsize',20)
83 - ylim([-50 900])
84 - set(gca,'FontSize',16)
85 - ylabel('Pull-off force [mN]','fontsize',16)
86 - xlabel('Time [s]','fontsize',16)
87
88 % On PDMS
89 - subplot(1,2,2)
90 - m=58; % test nr.
91 - plot(t,Adh(m).force_z)
92 - title('Pull-off on PDMS','fontsize',20)
93 - ylim([-50 200])
94 - set(gca,'FontSize',16)
95 - ylabel('Pull-off force [mN]','fontsize',16)
96 - xlabel('Time [s]','fontsize',16)
97
98
99 %% Load adhesion force data
100
101 - load('selecteddata_man_ad.mat'); % file containing the max. pull-off force per experiment (manually extracted)
102 - selecteddata = transpose(selecteddata man ad); % rows correspond with the experiment conditions, columns with the repetitions

```

```

103
104
105 %% Separate force data on glass and PDMS
106
107 % Extract the names of all unique experiment conditions
108 for i = 1:length(Adh)
109     M = strsplit(Adh(i).name, '_'); % split name in parts;
110     List(i,1) = strrep(string(strjoin(M(1:(3)))),' ','_');
111 end
112 List = unique(List); % rows of variables 'List' & 'selecteddata' correspond with each other
113
114 % Testdata on glass
115 w=1;
116 for i = 1:length(List)
117     if contains(List(i),'gls')
118         plotdata1(:,w)=selecteddata(:,i);
119         plotname1(w,:)= strsplit(List(i),'_');
120         w=w+1;
121     end
122 end
123 plotname1(4,1)='flat';
124
125 % Testdata on PDMS
126 w=1;
127 for i = 1:length(List)
128     if contains(List(i),'pdm')
129         plotdata2(:,w)=selecteddata(:,i);
130         plotname2(w,:)=strsplit(List(i),'_');
131         w=w+1;
132     end
133 end
134 plotname2(4,1)='flat';
135
136

```

```

137 %% Generate boxplots of max. pull-off forces
138
139 % On glass
140 figure(2);
141 subplot(1,2,1)
142 boxplot(plotdata1,plotname1(:,1))
143 title('Glass','fontsize',20)
144 ylim([0 110])
145 set(gca,'YTick',[0:10:110],'YGrid','on','XGrid','off','FontSize',16)
146 ylabel('Pull-off force [mN]','fontsize',16)
147
148 % On PDMS
149 subplot(1,2,2)
150 boxplot(plotdata2,plotname2(:,1))
151 title('PDMS','fontsize',20)
152 ylim([0 110])
153 set(gca,'YTick',[0:10:110],'YGrid','on','XGrid','off','FontSize',16)
154 ylabel('Pull-off force [mN]','fontsize',16)
155
156
157 %% Anova Grouping
158
159 for i = 1:length(Adh)
160     N = strsplit(Adh(i).name,'_');
161     Patt_name{i} = N{1,1};           % surface pattern
162     Subs_name{i} = N{1,2};         % substrate
163 end
164
165 % anova-n test
166 Data_vector = [plotdata1(:,1);plotdata2(:,1);plotdata1(:,2);plotdata2(:,2);plotdata1(:,3);plotdata2(:,3);plotdata1(:,4);plotdata2(:,4)]; % data vector
167 [PVal,Tbl,Stats,Terms]=anovan(Data_vector,{Patt_name,Subs_name},'model','full');
168
169 figure()
170 [C,M,H,Gnames] = multcompare(Stats,'Dimension',[1,2]);

```



## S.2.4 Data analysis – friction

The MATLAB-script that is used to process the friction data is inserted below.

```
1 % Processing friction data of adhesives with 4 pattern geometries against
2 % substrates with 2 stiffnesses
3 % Babette Haitzma Mulier, Peter van Assenbergh
4 % February 2020
5
6 % This scripts reads data-files that include friction and adhesion forces
7 % of micropatterned samples against hemispherical substrates. This data is
8 % obtained on a customized setup.
9
10 clear all
11 close all
12 clc
13
14
15 %% Load files
16
17 load('datalist.mat') % the general properties of the friction and adhesion data (names, etc.)
18 load('data.mat') % the friction and adhesion data; columns correspond with the names in 'datalist.mat'
19 load('k_char_fr.mat') % characterization matrix for friction: converts displacement into forces
20
21 t=(1:20000)/1000; % Time [s]
22
23
24 %% Filter/smoothen and level the data & store the info in variables
25
26 e= 10; %filter at this frequency (1/e = 0.1 sec)
27 o= 2000; %sampling frequency
28 [B,A] = butter(2,e/(o/2),'low'); % /2 nyquist correction; high/low: remove data above/below 'e' Hz
29
30 for i = 1:length(files)
31 N = strsplit(files(i).name, '_'); % split name in parts;
32 UsedData(i).displacement = data.raw(:,i); % get corresponding displacement data
33 UsedData(i).leveled = data.raw(:,i)-mean(data.raw(1:300,i)); % subtract the initial displacement-value, for comparison among all experiments
34 UsedData(i).filtered = filtfilt(B,A,UsedData(:,i).leveled);
```

```

35 -     UsedData(i).names = files(i).name;           % removes auto generated time stamp from the name of the data
36 -     UsedData(i).pattern = N{1};
37 -     UsedData(i).substrate = N{2};
38 -     UsedData(i).test = N{3};
39 -     UsedData(i).repetition= N{4};
40 -     UsedData(i).signal = N{5};
41 - end
42
43
44 - %% Extracting friction displacement data
45
46 - % Data in x-direction
47 - j=1;
48 - for i = 1:length(UsedData)
49 -     if contains(UsedData(i).names, 'fr')*contains(UsedData(i).names, '_x') == 1
50 -         Fri(j).name = UsedData(i).names;
51 -         Fri(j).filt_x = UsedData(i).filtered;
52 -         j=j+1;
53 -     end
54 - end
55
56 - % Data in z-direction
57 - j=1;
58 - for i = 1:length(UsedData)
59 -     if contains(UsedData(i).names, 'fr')*contains(UsedData(i).names, '_z') == 1
60 -         Fri(j).filt_z=UsedData(i).filtered;
61 -         j=j+1;
62 -     end
63 - end
64
65
66 - %% Convert displacement data to force data & extract peak forces friction
67
68 - for i = 1:length(Fri)

```

```

69 - Fri(i).force_x = Fri(i).filt_z * k_char_fr(1,1) + Fri(i).filt_x * k_char_fr(2,1); % x-direction
70 - Fri(i).force_z = Fri(i).filt_z * k_char_fr(1,2) + Fri(i).filt_x * k_char_fr(2,2); % z-direction
71 - Fri(i).max = abs(min(Fri(i).force_x)); % Peak force friction
72 - end
73
74
75 %% Representative friction force curves in time
76
77 % On glass
78 figure(1);
79 subplot(1,2,1)
80 m=10; % testnr. (d40s20)
81 plot(t,-Fri(m).force_x)
82 title('Friction on glass','fontsize',20)
83 ylim([-150 850])
84 set(gca,'YTick',[-150:100:850],'FontSize',16)
85 ylabel('Friction force [mN]','fontsize',16)
86 xlabel('Time [s]','fontsize',16)
87
88 % On PDMS
89 subplot(1,2,2)
90 m=12; % test nr. (d40s20)
91 plot(t,-Fri(m).force_x)
92 title('Friction on PDMS','fontsize',20)
93 ylim([-50 250])
94 set(gca,'YTick',[-50:50:250],'FontSize',16)
95 ylabel('Friction force [mN]','fontsize',16)
96 xlabel('Time [s]','fontsize',16)
97
98
99 %% Load friction force data
100
101 load('selecteddata_man_fr.mat'); % file containing the max. friction force per experiment (manually extracted)
102 selecteddata = transpose(selecteddata man fr); % rows correspond with the experiment conditions, columns with the repetitions

```

```

103
104
105 %% Separate force data on glass and pdms
106
107 % Extract the names of all unique experiment conditions
108 - for i = 1:length(Fri)
109 -     M = strsplit(Fri(i).name, '_');           % split name in parts;
110 -     List(i,1) = strrep(string(strjoin(M(1:(3)))), ' ', '_');
111 - end
112 - List = unique(List);                       % rows of variables 'List' & 'selecteddata' correspond with each other
113
114 % Testdata on glass
115 - w=1;
116 - for i = 1:length(List)
117 -     if contains(List(i), 'gls')
118 -         plotdata1(:,w)=selecteddata(:,i);
119 -         plotname1(w,:)= strsplit(List(i), '_');
120 -         w=w+1;
121 -     end
122 - end
123 - plotname1(4,1)='flat';
124
125 % Testdata on PDMS
126 - w=1;
127 - for i = 1:length(List)
128 -     if contains(List(i), 'pdm')
129 -         plotdata2(:,w)=selecteddata(:,i);
130 -         plotname2(w,:)=strsplit(List(i), '_');
131 -         w=w+1;
132 -     end
133 - end
134 - plotname2(4,1)='flat';
135
136

```

```

137 %% Generate boxplots of max. friction force
138
139 % On glass
140 figure(2)
141 subplot(1,2,1)
142 boxplot(plotdata1,plotname1(:,1))
143 title('Glass','fontsize',20)
144 ylim([0 700])
145 set(gca,'YTick',[0:50:700],'YGrid','on','XGrid','off','FontSize',16)
146 ylabel('Friction force [mN]','fontsize',16)
147
148 % On PDMS
149 subplot(1,2,2)
150 boxplot(plotdata2,plotname2(:,1))
151 title('PDMS','fontsize',20)
152 ylim([0 700])
153 set(gca,'YTick',[0:50:700],'YGrid','on','XGrid','off','FontSize',16)
154 ylabel('Friction force [mN]','fontsize',16)
155
156
157 %% Anova Grouping
158
159 for i = 1:length(Fri)
160     N = strsplit(Fri(i).name, '_');
161     Patt_name{i} = N{1,1};           % surface pattern
162     Subs_name{i} = N{1,2};         % substrate
163 end
164
165 % anova-n test
166 Data_vector = [plotdata1(:,1);plotdata2(:,1);plotdata1(:,2);plotdata2(:,2);plotdata1(:,3);plotdata2(:,3);plotdata1(:,4);plotdata2(:,4)]; % data vector
167 [PVal,Tbl,Stats,Terms]=anovan(Data_vector,{Patt_name,Subs_name},'model','full');
168
169 figure()
170 [C,M,H,Gnames] = multcompare(Stats,'Dimension',[1,2]);
171
172
173 %% Anova1 - check
174
175 [PVa2,Tb2,Stats2]=anova1(plotdata2,plotname2(:,1).');
176
177 figure()
178 [C2,M2,H2,Gnames2] = multcompare(Stats2,'Dimension',[1,2]); % add or remove levels to plot different effects.

```